BIOCHEMISTRY

Light-activated molecular machines are fast-acting broad-spectrum antibacterials that target the membrane

Ana L. Santos[1,2]*†, Dongdong Liu[1]†, Anna K. Reed[1], Aaron M. Wyderka[1], Alexis van Venrooy[1], John T. Li[1], Victor D. Li[1], Mikita Misiura[1], Olga Samoylova[1], Jacob L. Beckham[1], Ciceron Ayala-Orozco[1], Anatoly B. Kolomeisky[1], Lawrence B. Alemany[1,3], Antonio Oliver[2,4], George P. Tegos[5], James M. Tour[1,6,7,8]*

The increasing occurrence of antibiotic-resistant bacteria and the dwindling antibiotic research and development pipeline have created a pressing global health crisis. Here, we report the discovery of a distinctive antibacterial therapy that uses visible (405 nanometers) light-activated synthetic molecular machines (MMs) to kill Gram-negative and Gram-positive bacteria, including methicillin-resistant *Staphylococcus aureus*, in minutes, vastly outpacing conventional antibiotics. MMs also rapidly eliminate persister cells and established bacterial biofilms. The antibacterial mode of action of MMs involves physical disruption of the membrane. In addition, by permeabilizing the membrane, MMs at sublethal doses potentiate the action of conventional antibiotics. Repeated exposure to antibacterial MMs is not accompanied by resistance development. Finally, therapeutic doses of MMs mitigate mortality associated with bacterial infection in an in vivo model of burn wound infection. Visible light–activated MMs represent an unconventional antibacterial mode of action by mechanical disruption at the molecular scale, not existent in nature and to which resistance development is unlikely.

INTRODUCTION

Antimicrobial resistance (AMR) represents one of the greatest challenges facing humankind (*1*). AMR is currently responsible for 700,000 deaths/year (*2*). By 2050, 10 million lives/year worldwide will be at risk from drug-resistant infections (*3*).

While long-established classes of conventional antibiotics are becoming increasingly ineffective against a growing number of drug-resistant pathogens, the development of new antimicrobial agents has nearly stagnated. No new class of antibiotics against Gram-negative bacteria has been approved since the late 1980s (*4*), and only one in four antibiotics under clinical development is a novel drug class or acts via a new mechanism of action (*5*). This makes most antibiotics under development susceptible to the same resistance mechanisms of previously developed molecules. There is, therefore, an urgent global need to develop safe and effective new antimicrobials that limit the rise of bacterial resistance while preserving the viability of existing antibiotics.

Over the past decade, antimicrobial nanomaterials that are novel to bacteria and thus are not a priori within their natural defensive arsenal have gained increasing attention as an emerging "outside-the-box" approach against antibiotic-resistant bacteria (*6*, *7*). Stimuli-activated, "smart" nanomaterials are particularly appealing antimicrobials due to the ability to precisely control their activities in time and/or in space, mitigating detrimental side effects to human cells (*8*).

Synthetic molecular motors, or molecular machines (MMs), are molecular structures that can rotate unidirectionally in a controlled manner in response to stimuli, resulting in a mechanical action (*9*). Among the stimuli that can activate MMs, light is particularly appealing because of its nonchemical and noninvasive nature and ease of control. Synthetic MMs consist of a stator and a light-activated rotor (Fig. 1A). Following irradiation, the molecule undergoes successive unidirectional rotation, resulting in a drilling-like rapid (≈3 MHz) motion (Fig. 1B) that can propel it through a lipid bilayer (Fig. 1C) (*10*). MMs show great promise in a multitude of applications, from drug delivery to chemo- and antimicrobial therapy (*9*, *11*, *12*). However, reliance on ultraviolet (UV) radiation for activation limits the clinical utility of previously developed MMs due to the detrimental effects of these wavelengths to mammalian cells (*13*).

Here, we describe six visible light (405 nm)–activated MMs that kill Gram-negative and Gram-positive bacteria, including methicillin-resistant *Staphylococcus aureus* (MRSA), in as little as 2 min of light activation without detectable resistance. This unconventional antimicrobial therapy is effective not only against exponentially growing planktonic cells but also resistant phenotypes, such as biofilms and persister cells. Using electron microscopy, RNA sequencing (RNA-seq), and spectrophoto- and spectrofluorimetric methods, the mode of action of MMs was found to involve mechanical disruption of the membrane, leakage of intracellular material, and loss of membrane potential. In addition, sublethal treatment with MMs potentiated the action of conventional antibiotics as a result of MM-induced membrane permeabilization and enhanced antibiotic access to intracellular targets. Last, at therapeutic levels, MMs mitigated mortality associated with infection by different bacterial strains (*Acinetobacter baumannii* and *S. aureus*) in a burn wound infection model.

[1]Department of Chemistry, Rice University, Houston, TX 77005, USA. [2]IdISBA–Fundación de Investigación Sanitaria de las Islas Baleares, Palma, Spain. [3]Shared Equipment Authority, Rice University, Houston, TX 77005, USA. [4]Servicio de Microbiologia, Hospital Universitari Son Espases, Palma, Spain. [5]Office of Research, Reading Hospital, Tower Health, 420 S. Fifth Avenue, West Reading, PA 19611, USA. [6]Smalley-Curl Institute, Rice University, Houston, TX 77005, USA. [7]Department of Materials Science and NanoEngineering, Rice University, Houston, TX 77005, USA. [8]NanoCarbon Center and the Welch Institute for Advanced Materials, Rice University, Houston, TX 77005, USA.
*Corresponding author. Email: alsantos@ua.pt (A.L.S.); tour@rice.edu (J.M.T.)
†These authors contributed equally to this work.

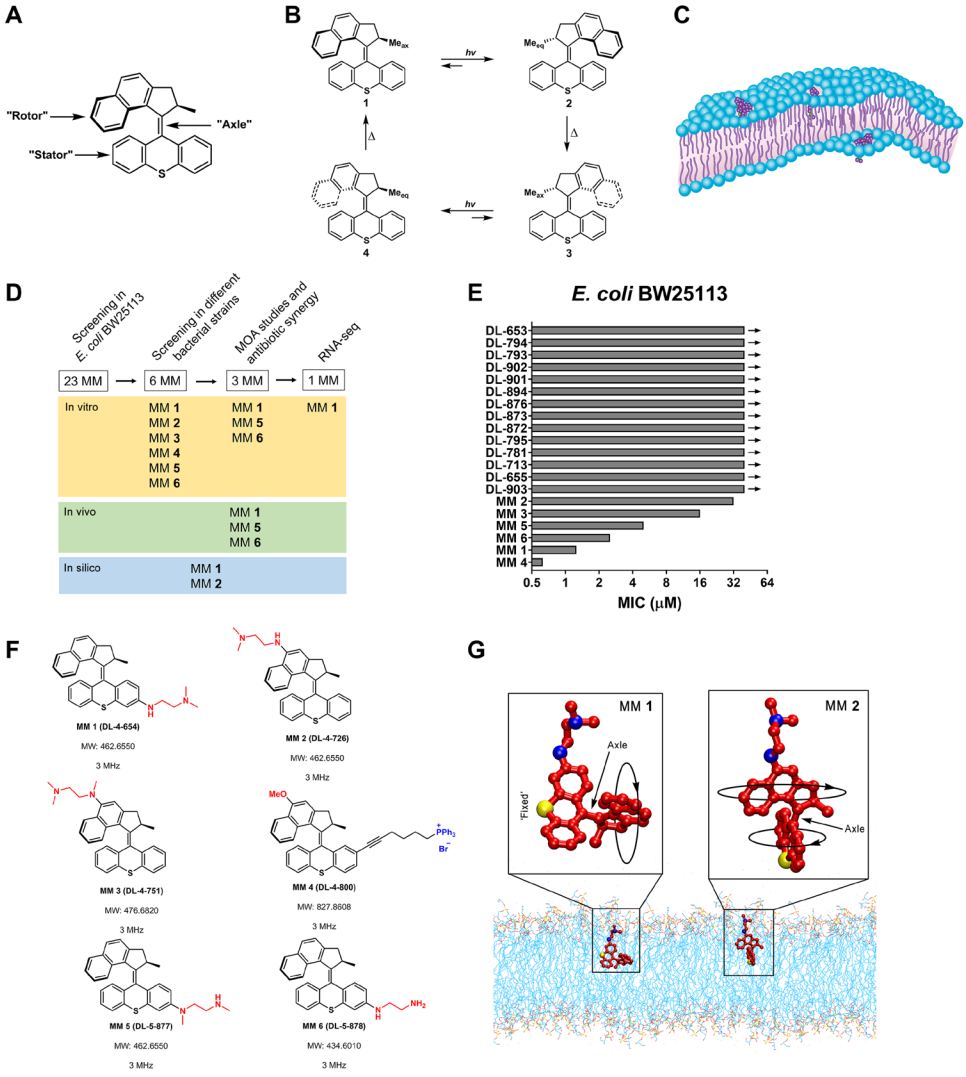

Fig. 1. MMs as antibacterials. (**A**) General structure of an MM. (**B**) Rotation cycle of an MM. Photoisomerization of the MMs (**1** → **2**) generates the metastable conformer, **2**. Following the thermal helix inversion step (**2** → **3**), during which the methyl group moves from the pseudo-equatorial to pseudo-axial position and the naphthalene moiety in the rotor moves behind the stator, a second stable conformer, **3**, is generated. A subsequent photoisomerization step (**3** → **4**) and corresponding thermal helix inversion (**4** → **1**) generate the full 360° rotation cycle. (**C**) Schematic representation of an MM drilling through the cell membrane as would occur following light activation. (**D**) Overview of the workflow used in this study and the different MMs examined at each step. MOA, mechanism of action. (**E**) MIC value of different MMs in *E. coli* BW25113. Arrows next to the bars denote that the MIC value was higher than the maximal concentration (40 μM) tested. Bars represent the results from at least three biological replicas. (**F**) Chemical structure of the antibacterial MMs identified in this study. Functional groups highlighted in red, and blue were introduced to tune the activation wavelength of the motor and increase water solubility, respectively. MW, molecular weight. (**G**) Schematic representation of the different positioning of MM **1** and MM **2** in the bacterial membrane based on results from molecular dynamics simulations.

MMs represent a distinctive stimuli-activated antibacterial therapy whose mechanism is based on mechanical action at the molecular scale. This unique mechanism of action is unlike that of any other antibacterial compound, and the development of resistance to MMs is unlikely.

RESULTS

MMs are fast-acting broad-spectrum antibacterials

A library of 19 different visible light–activated (405 nm) MMs displaying fast rotation rates (≈3 MHz) was synthesized (table S1). Visible light activation (fig. S1) was achieved by introducing an amine or alkoxy electron–donating substituent into the conjugated core of the MMs. The molecules were further modified with different amines in either the stator or the rotor portion of the molecule to promote the association between the protonated amines of the MMs and the negatively charged bacterial membrane.

This MM library was originally screened for antibacterial activity in *Escherichia coli* BW25113 (Fig. 1D). *E. coli* cell suspensions were incubated with a range of concentrations (0.3125 to 40 μM) of the different MMs [8 mM stock in dimethyl sulfoxide (DMSO)] and then irradiated for 5 min with 405-nm light at 146 mW cm^{-2} (43.8 J cm^{-2}). DMSO-only controls were included in every experiment to exclude possible effects of the vehicle. Irradiated cell suspensions were collected

and inoculated into cation-adjusted Mueller-Hinton broth (MHB). Following overnight incubation (37°C), samples were inspected for growth. The minimal inhibitory concentration (MIC) of light-activated MMs was defined as the concentration of MMs resulting in no visible bacterial growth following irradiation with 43.8 J cm^{-2} of 405-nm light (fig. S2).

The MIC of the different MMs in *E. coli* is shown in Fig. 1E. Six fast-rotating MMs (MM **1** to MM **6**) (Fig. 1F) displaying MIC values within the range of concentrations tested were identified. MM **4**, characterized by the presence of a triphenylphosphonium (TPP^+) group, displayed the lowest MIC in *E. coli* (0.625 μM), closely followed by MM **1** (1.25 μM). MM **2**, characterized by the presence of a tertiary amine on the side chain of the rotor portion of the molecule, displayed the highest MIC (32 μM). Slow rotating MM controls (≈10^{-3} Hz) (table S1) did not exhibit antibacterial activity (fig. S3), denoting the importance of fast rotation rates for the antibacterial properties of MMs. However, substantial differences in rotation rates of the different antibacterial MMs were not detected (fig. S4), suggesting that small variations in the rotation rate of fast MMs cannot explain differences in their antibacterial activity.

Molecular dynamics simulations revealed substantial differences in the distributions of angles between the MM axle and the plane of the membrane of the most potent (MM **1**) and the least potent (MM **2**) antibacterial MMs (fig. S5). In the case of MM **1**, the axle of the molecule is close to parallel to the membrane (average angle of ≈15°), while for MM **2**, the axle is more perpendicular to the membrane (average angle of ≈60°) (fig. S5A). These observations indicate that MM **1** and MM **2** adopt distinct equilibrium configurations when bound to the lipid bilayer membrane (Fig. 1G) as a result of the different placement of the positively charged tertiary amine group in MM **1** and MM **2**. Equilibrium simulations also revealed that the axle of MM **1** can penetrate about 2 Å deeper into the membrane than that of MM **2**, denoted by the slight left shift of the histogram of the distributions of distances between geometric centers of axles of the MMs and membrane center of MM **1** relatively to MM **2** (fig. S5B). This is also supported by the finding that the potential of mean force (PMF) curve for MM **1** is lower and slightly to the left of the PMF curve of MM **2** (fig. S6), suggesting that it is more favorable for MM **1** to be located deeper inside the membrane. These differences in orientation and positioning of the two molecules within the membrane, and subsequent differences in the way they rotate following light activation, might influence the extent of the membrane deformation they exert and thus account for their distinct antibacterial activities.

The bacteriostatic potential of the identified MMs (Fig. 1F) was further investigated in additional Gram-negative and Gram-positive bacterial strains (tables S2 and S3). Killing by light-activated MMs varied in a concentration- and light intensity–dependent manner, with enhanced MM concentration and light intensity resulting in higher MM-induced killing (fig. S7). Some toxicity of the MM itself (in the absence of light) was detected, particularly for the TPP^+ containing MM **4** (fig. S7), which was, therefore, excluded in subsequent "mode-of-action" experiments. Among the strains tested, *S. aureus* was particularly susceptible to killing by high MM concentrations even in the absence of light. *S. aureus* also exhibited substantial sensitivity to 405-nm light alone (fig. S7). Light dose–dependent reduction of bacterial numbers by different concentrations of the most potent MMs (MM **1**, MM **5**, and MM **6**) revealed that complete eradication of *A. baumannii* and *E. coli* required at least 40 J cm^{-2} of 405-nm light in samples treated with the highest concentration of MMs tested (5 μM). Complete eradication of *Pseudomonas aeruginosa* and *S. aureus* could be achieved with 16 J cm^{-2} of 405-nm light and 0.625 to 5 μM of MMs (fig. S8).

The bactericidal properties of MMs (2× MIC) were further examined at a fixed light intensity of 146 mW cm^{-2} (Fig. 2A and table S4). In *A. baumannii*, treatment with different MMs reduced cell number to the limit of detection in 3 min (MM **4**) to 10 min (MM **3**). In *E. coli*, bacterial numbers were reduced to the limit of detection in 4 min (MM **4**, MM **5**, and MM **6**) to 10 min (MM **2**) of irradiation in the presence of 2× MIC of each MM. For *P. aeruginosa*, MM-induced reduction of cell numbers to the limit of detection was achieved in 3 min (MM **1** and MM **4**) to 10 min (MM **3** and MM **6**). Complete elimination of *S. aureus* was achieved in 2 min (MM **4**) to 4 min (MM **2** and MM **3**) of irradiation.

The antibacterial spectrum of action of the most efficient MMs (MM **1**, MM **5**, and MM **6**) was assessed in additional strains, including MRSA (Fig. 2B). The MIC of MM **1** ranged from 0.078 μM in *Bacillus megaterium* and *Staphylococcus epidermidis* to 10 μM in *Burkholderia cepacia* and *Bacillus cereus*. The MIC of MM **5** ranged from 0.078 μM in *B. megaterium*, *S. aureus*, and *S. epidermidis* to 20 μM in *B. cepacia* and *Enterobacter cloacae*. The MIC of MM **6** ranged from 0.078 μM in *S. aureus* and *S. epidermidis* to 10 μM in *B. cepacia*, *B. cereus*, and *E. cloacae*. Overall, while the median MIC of MM **5** in Gram-positive bacteria was lower than that in Gram-negative bacteria ($P < 0.05$), in the case of MM **1** and MM **6**, significant differences in the MIC between the two bacterial groups were not observed (Fig. 2C).

The antibacterial properties of MMs were also assessed in a panel of *E. coli* single-gene knockouts, deleted for genes encoding different components of efflux pumps responsible for resistance to different antibiotics (table S5). The MIC of the different single-gene knockouts was lower, equal, or superior to that of the wild-type parent strain depending on the gene deleted, with no particular trend toward resistance or sensitivity to MM treatment among the panel of strains tested (fig. S9).

MMs kill persister cells and disrupt established biofilms

The ability of light-activated MMs (1× MIC) to kill antibiotic-tolerant persister cells (Fig. 3A) was investigated in the Gram-negative strains *A. baumannii*, *E. coli*, and *P. aeruginosa*. In *S. aureus*, stationary phase cells were used in persister eradication assays (*14*). In *A. baumannii*, treatment with MMs resulted in a reduction in the levels of persisters to the limit of detection in 3 min (MM **1**) to 15 min (MM **3**) of irradiation. The number of persister cells of *E. coli* was reduced to the limit of detection in 5 min (MM **2**, MM **4**, and MM **6**) to 10 min (MM **1**, MM **5**, and MM **3**) of irradiation. In the case of *P. aeruginosa*, persister levels were reduced to the limit of detection in 2 min (MM **1**) to 15 min (MM **2**) of irradiation. Reduction in the number of persister cells of *S. aureus* to the limit of detection was achieved in 3 min (MM **2** and MM **4**) to 10 min (MM **3**) (Fig. 3A).

The antibiofilm potential of the most efficient MMs was investigated in a 96-well plate format using a combination of methods targeting different components of the biofilm (*15*). Since preliminary experiments revealed that, for the same irradiation period, treatment with 1× or 2× MIC of MMs resulted in a similar reduction in biofilm biomass (fig. S10); in subsequent experiments, irradiation time, rather than MM concentrations, was varied.

Mature biofilms of *P. aeruginosa* and *S. aureus* were established and then challenged with 1% DMSO or 2× MIC of MM **1**, MM **5**, and

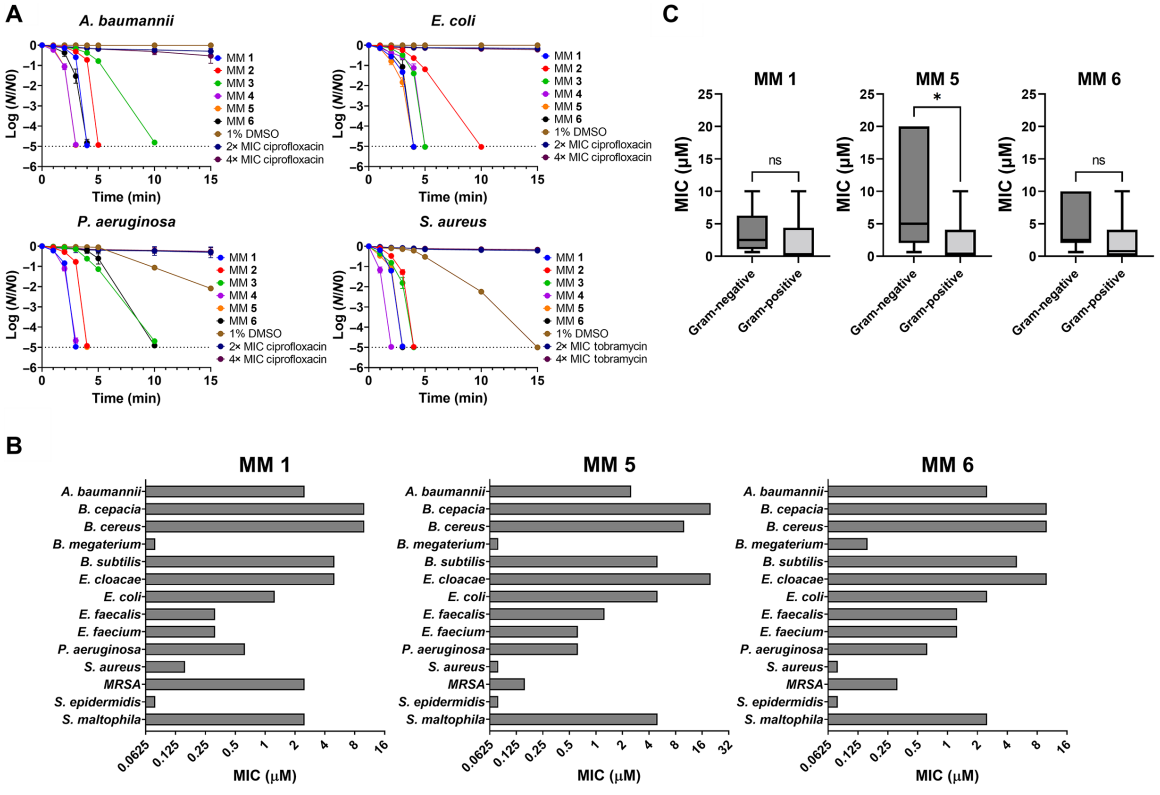

Fig. 2. MMs are fast-acting, broad-spectrum antibacterials. (**A**) Time-dependent reduction in the abundance of different exponentially growing bacterial strains in the presence of 1% DMSO or 2× MIC of each MM and 146 mW cm^{-2} of 405-nm light, or 2× and 4× the MIC of conventional antibiotics. The dotted line denotes the limit of detection of the method. Results are the means of at least three biological replicas ± standard error of the mean. (**B**) MIC value of MM **1**, MM **5**, and MM **6** in different Gram-negative and Gram-positive strains, including MRSA. Bars represent the results from at least three biological replicas. Unless otherwise noted, results for MMs and DMSO are always reported in the presence of light. (**C**) Box and whiskers plot (median values with min/max range) of the MIC values of MM **1**, MM **5**, and MM **6** among the Gram-negative and Gram-positive strains examined in this study. *$P < 0.05$; ns, not significant.

MM **6**, followed by 405-nm irradiation at 146 mW cm^{-2} for 15, 30, and 45 min. Conventional antibiotics (rifampin and tobramycin) at 2× MIC were used as controls. The effect of visible light–activated MMs on total bacterial cell number within biofilms was assessed using the nucleic acid dye acridine orange (*15*). Compared to untreated controls, treatment with the antibiotics tobramycin and rifampin resulted in a reduction in total bacterial cell numbers of up to 43 and 64% ($P < 0.01$), respectively. DMSO-treated samples showed a reduction in total cell numbers of up to 50% ($P < 0.01$), while MM-treated cells showed up to 78% ($P < 0.01$) reduction in total cell number, compared to the respective untreated controls (Fig. 3B).

Adenosine 5′-triphosphate (ATP) quantification was used as a proxy of the number of metabolically active cells within biofilms (*15*). The population of metabolically active cells was reduced from 18 to 27% ($P < 0.05$) by rifampin and tobramycin, respectively, even after 45 min of treatment, while a 15-min treatment period with visible light–activated MMs reduced the amount of metabolically active cells by as much as 94% ($P < 0.01$), compared to a 66% reduction ($P < 0.01$) in DMSO-treated samples, relatively to the respective untreated controls (Fig. 3C).

Treatment with control antibiotics resulted in a reduction in biofilm protein content of up to 78% ($P < 0.01$). The same treatment time resulted in up to 82% reduction ($P < 0.01$) in biofilm protein in DMSO-treated samples and up to 89% reduction ($P < 0.01$) in MM-treated samples, compared to untreated controls (Fig. 3D).

Treatment with the antibiotics tobramycin and rifampin resulted in a reduction of biofilm biomass of up to 29% (Fig. 3E). Compared to untreated controls, treatment with visible light–activated MMs resulted in a biomass reduction of up to 99% ($P < 0.05$), while DMSO-treated samples showed a reduction in biofilm biomass of up to 49% (Fig. 3E).

Repeated exposure to MMs does not lead to the development of resistance

The ability of cells to develop resistance to successive MM exposure was assessed by serial passaging, whereby cells surviving treatment with 0.5× MIC of the different MMs followed by 5 min of irradiation with 405-nm light at 146 mW cm^{-2} (43.8 J cm^{-2}) were collected and subjected to 20 cycles of repeated exposure to MMs. Repeated exposure to MMs did not result in a change in the MIC, in contrast to the steep increase (32- to 128-fold) in the MIC through time that was observed in samples treated with conventional antibiotics (Fig. 3F). Mutants that evolved resistance to antibiotics did not exhibit cross-resistance to MMs (table S6).

MMs target the cell membrane

The mechanism of action of MMs was investigated using RNA-seq, an array of spectrophoto- and spectrofluorimetric methods, and

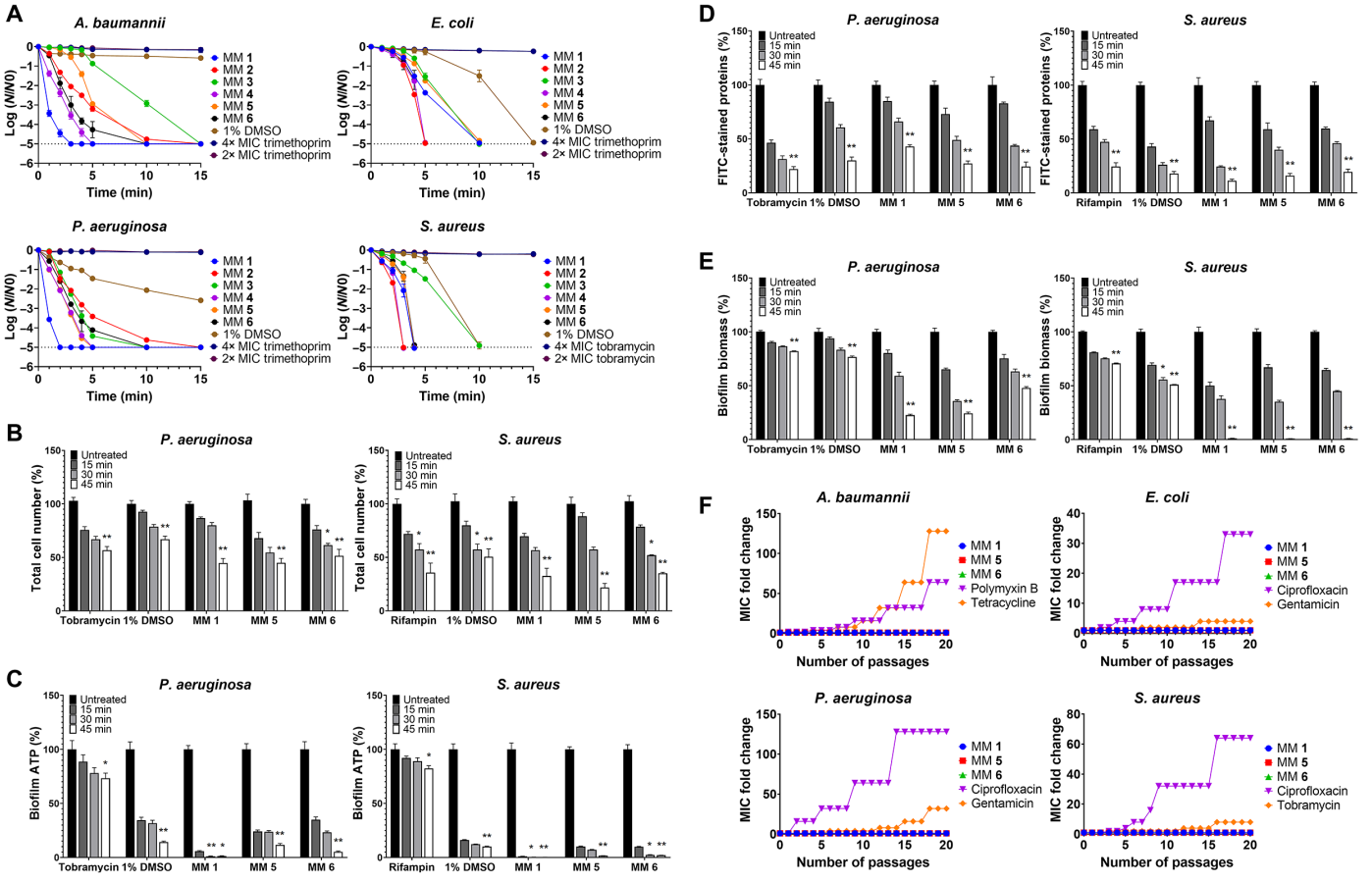

Fig. 3. MMs eliminate persisters and biofilms without detectable resistance. (**A**) Time-dependent reduction in the abundance of persister cells of different bacterial strains in the presence of 1% DMSO or 1× MIC of each MM and 405-nm light at 146 mW cm^{-2} or 2× and 4× the MIC of conventional antibiotics. The dotted line denotes the limit of detection of the method. Reduction in (**B**) total bacterial cell number assessed using acridine orange, (**C**) metabolically active cells assessed from ATP levels, (**D**) total protein assessed using fluorescein isothiocyanate (FITC) fluorescence, and (**E**) total biomass assessed using crystal violet in established biofilms of *P. aeruginosa* and *S. aureus*, following irradiation (146 mW cm^{-2} of 405-nm light) for different time periods in the presence of 1% DMSO or 2× MIC of MMs or in the presence of 2× MIC of conventional antibiotics. Results are shown as the mean of at least three biological replicas ± standard error of the mean. (**F**) MIC fold change relative to the original MIC following repeated exposure to MMs and control antibiotics. Results are shown as the average of at least three biological replicas. Unless otherwise noted, results for MMs and DMSO are always reported in the presence of light. *$P < 0.05$; **$P < 0.01$.

electron microscopy (Fig. 1D). All mechanism of action studies were conducted under the same irradiation conditions: 5 min of irradiation with 405-nm light at 146 mW cm^{-2} (light dose of 43.8 J cm^{-2}).

RNA-seq was conducted on *E. coli* treated with 0.5× MIC of the most potent MM (MM **1**) or 1% DMSO and 43.8 J cm^{-2} of 405-nm light (Fig. 4A). A total of 4311 transcripts were detected by RNA-seq (Fig. 4B). Of these, 2694 showed significantly different levels ($P <$ 0.05) in MM-treated cells compared to DMSO controls. A total of 1362 transcripts were significantly more abundant in MM-treated samples, while 1332 transcripts were significantly more abundant in DMSO controls. MM **1**–treated samples and DMSO controls exhibited distinct transcriptomic profiles (Fig. 4C), with some transcripts displaying as much as a fivefold difference in abundance between treatments (Fig. 4D).

Gene ontology (GO) enrichment analysis revealed that transcripts more abundant in DMSO controls were significantly enriched ($P <$ 0.05) for membrane-associated biological processes and molecular functions, including respiration and transmembrane transport (tables S7 and S8). Transcripts more abundant in DMSO controls were also significantly enriched ($P < 0.05$) for membrane-related cellular components (table S9).

Analysis of transcripts significantly more abundant in MM-treated cells did not reveal a significant enrichment for particular biological processes, molecular functions, or cellular components, denoting the unspecific character of MM-induced cellular damage. To further understand whether the genes encoding the transcripts more abundant in MM-treated samples compared to DMSO controls play a role in susceptibility to MMs, the MIC for the corresponding single-gene knockouts (table S10) was assessed. No consistent trend toward resistance or sensitivity to MM treatment was observed (fig. S11), suggesting no particular relevance of these genes to the cell's response to MMs.

On the basis of the results obtained by RNA-seq identifying the membrane as the major target of MMs, the investigation into the mode of action of MMs proceeded by examining their impact on inner and outer membrane integrity. The fluorescent probe *N*-phenyl-1-naphthylamine (NPN) was used to examine damage to the

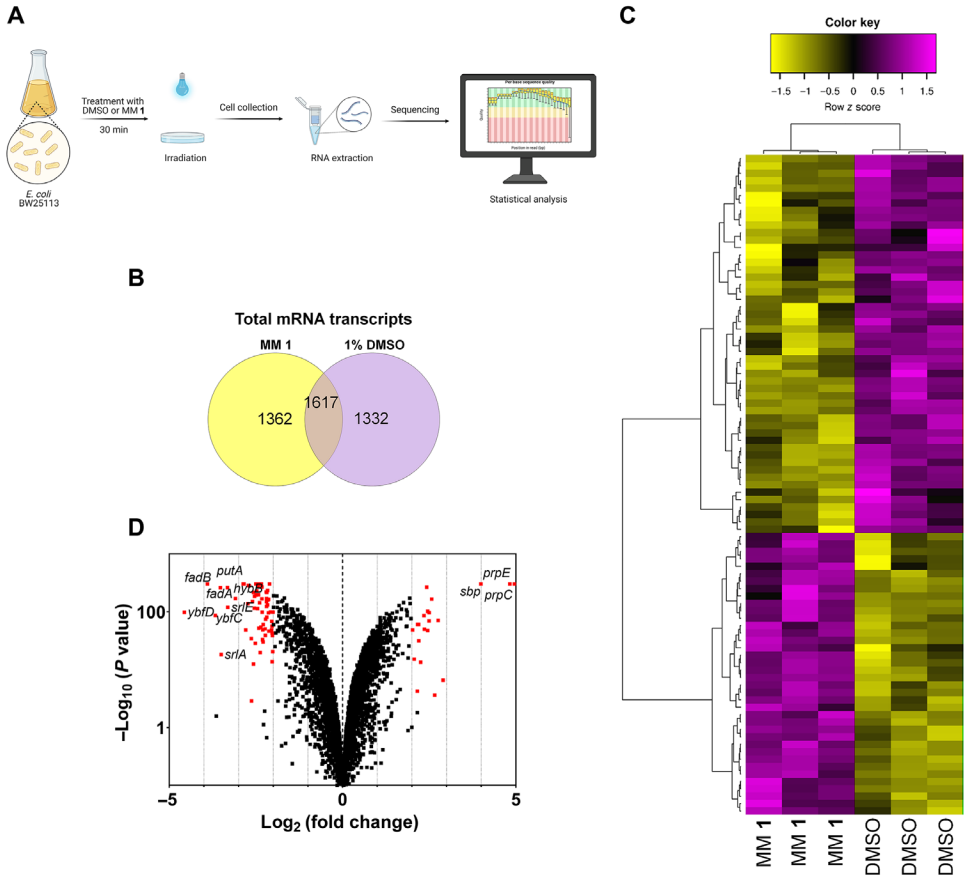

Fig. 4. MM- and DMSO-treated cells display distinct transcriptomic profiles. (**A**) RNA-seq workflow created with Biorender.com. (**B**) Venn diagram of the transcriptomic profiles of MM- and DMSO-treated samples. (**C**) Heatmap representation of *z* scores for gene transcripts displaying an adjusted $P < 0.01$ and the highest fold change in abundance in MM- and DMSO-treated samples. (**D**) Volcano plot of statistically significant ($P < 0.05$) differentially expressed genes identified from the RNA-seq libraries. Results are the average of three biological replicas.

outer membrane (*16*). Treatment of *E. coli* with MMs and 43.8 J cm^{-2} of 405-nm light resulted in a concentration-dependent increase in NPN fluorescence by as much as 2.5-fold in the case of MM **6**, compared to DMSO controls (Fig. 5A), denoting MM-induced damage to the outer membrane of the cell.

The effect of treatment with MMs in inner membrane permeability was examined by monitoring the fluorescence of propidium iodide (PI) in *E. coli* cells treated with different concentrations of each MM or DMSO in the presence and absence of 405-nm light (43.8 J cm^{-2}). Treatment with MMs (0.5 to 1× MIC) resulted in an overall increase in PI fluorescence (Fig. 5B), denoting damage to the inner membrane of the cell in MM-treated samples. Treatment with MMs also resulted in a significant increase in extracellular levels of ATP from 4.6×10^{-10} mol in dark DMSO controls up to 1.2×10^{-7} mol in cells challenged with 1× MIC of MM **1** (Fig. 5C), denoting leakage of intracellular contents following MM treatment.

Membrane damage was accompanied by dissipation of the membrane potential, denoted by an increase in 3,3′-dipropylthiadicarbocyanine iodide [$DiSC_3(5)$] fluorescence by as much as 1.9-, 1.6-, and 1.3-fold following treatment with 1× MIC of MM **1**, MM **5**, and MM **6**, respectively, compared to DMSO controls (Fig. 5D). Similar trends in terms of MM-induced membrane damage (fig. S12) and loss of membrane potential (fig. S13) were also observed in the Gram-positive *S. aureus*, demonstrating that the mechanism of action of MMs is not species specific.

Transmission electron microscopy (TEM) images revealed that treatment of *E. coli* with 0.5× MIC of MM **1**, MM **5**, and MM **6** and 43.8 J cm^{-2} of 405-nm light resulted in substantial changes in cell morphology, including the detachment of the inner membrane from the cell wall, damage to peptidoglycan, distortion of the cell surface, and formation of outer membrane vesicles denoting membrane and periplasmic stress (Fig. 5E). Scanning electron microscopy (SEM) showed that, compared to DMSO controls, samples treated with MM **1** displayed reduced cell size accompanied by deformation and wrinkling of the cell surface. MM-treated samples also exhibited multiple pore-like deformations throughout the cell surface, which were not detected in DMSO-treated cells (Fig. 5F).

MMs potentiate antibiotic action

The interaction of MMs with conventional antibiotics was investigated by determining the MIC of different classes of antibiotics alone and following treatment of *E. coli* with sub-MIC concentrations of visible light–activated MMs (Fig. 1D) using a modified checkerboard assay. In the case of the antibiotics gentamicin,

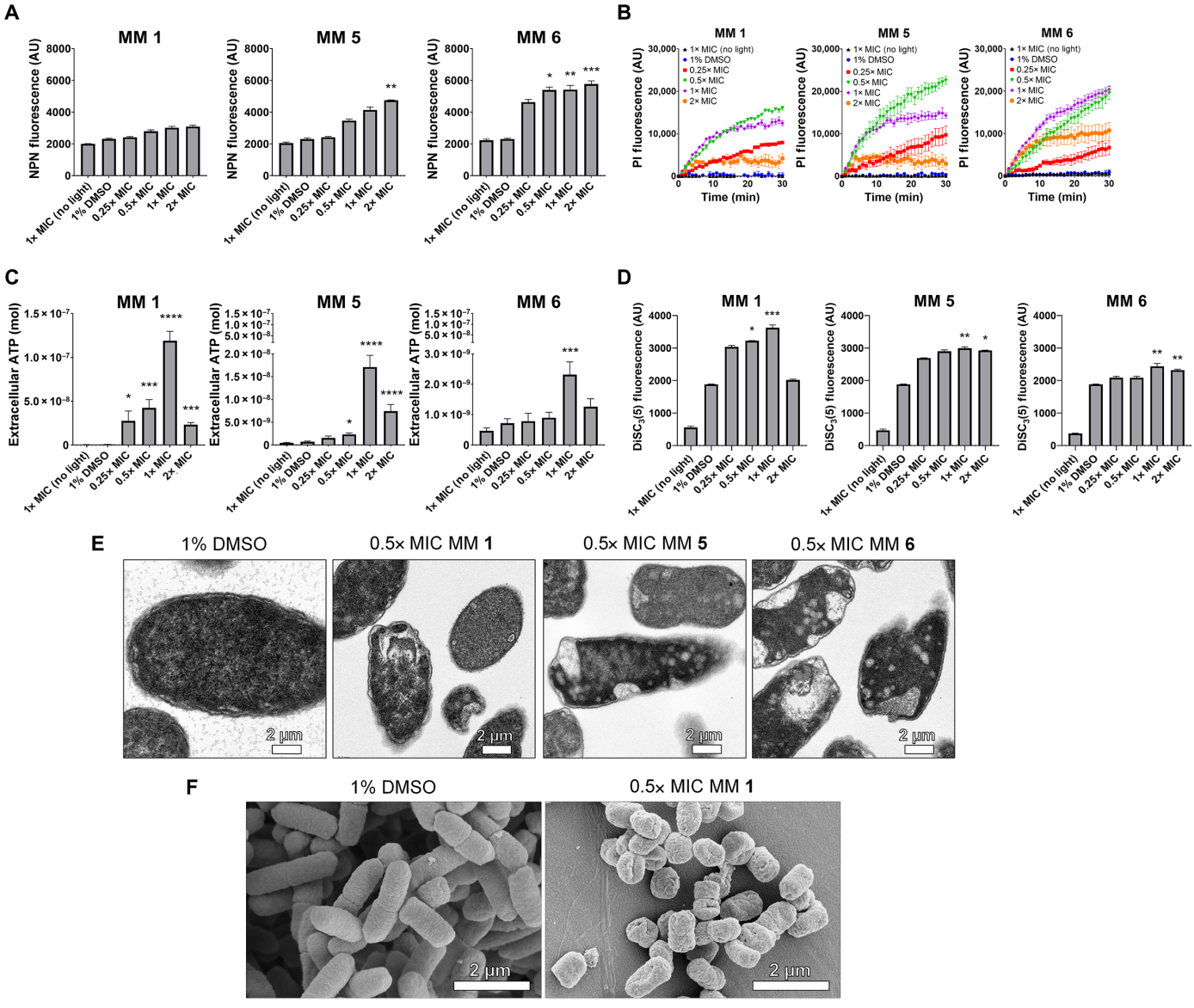

Fig. 5. Mechanisms of action of visible light–activated MMs. (**A**) Uptake of NPN by the *E. coli* outer membrane following treatment with 1% DMSO or different concentrations of MMs. AU, arbitrary units. (**B**) Time progression of PI fluorescence following treatment of *E. coli* with different concentrations of MMs or 1% DMSO. (**C**) Extracellular ATP levels following treatment of *E. coli* with 1% DMSO or different concentrations of MMs. (**D**) Fluorescence of the membrane potential probe 3,3-dipropylthiadicarbocyanine iodide [$DiSC_3(5)$] following treatment of *E. coli* with 1% DMSO or different concentrations of MMs. All results are shown as the means of at least three biological replicas ± standard error of the mean. (**E**) Transmission electron microscopy (TEM) images of *E. coli* treated with 1% DMSO or 0.5× MIC of MMs. (**F**) Scanning electron microscopy (SEM) images of *E. coli* treated with 1% DMSO or 0.5× MIC of MM **1**. Unless otherwise noted, results for MMs and DMSO are always reported in the presence of light. **P* < 0.05; ***P* < 0.01; ****P* < 0.001; *****P* < 0.0001.

ciprofloxacin, and ampicillin, pretreatment of cells with light-activated MMs resulted in a decrease in the antibiotic MIC value by two- to fourfold. In the case of the antibiotic novobiocin, the MIC value was markedly reduced from 0.48 μg ml^{-1} in untreated cells to 0.0075 μg ml^{-1} when cells were pretreated with MM **1** and MM **5** and to 0.015 μg ml^{-1} in the case of pretreatment with MM **6** (Fig. 6A). Calculation of the fractional inhibitory concentration (FIC) index (*17*) revealed a synergistic interaction between MMs and novobiocin (FIC index ≤ 0.5), suggesting potentiation (up to 64-fold) of the action of novobiocin by pretreatment with MMs (Fig. 6B).

The ability of MMs to potentiate antibiotic killing was further examined by pretreating cells with 0.5× MIC of MMs and 43.8 J cm^{-2} of 405-nm light before challenge with different antibiotics for 2 hours (Fig. 6C). On average, treatment of *E. coli* with 4× MIC of different antibiotic combinations resulted in a three-log reduction in bacterial numbers compared to treatment with individual antibiotics (Fig. 6D). However, cells that were pretreated with sublethal concentrations of MMs exhibited a four-log reduction in bacterial numbers following antibiotic challenge, compared to the treatment with individual antibiotics and antibiotic combinations. The observation

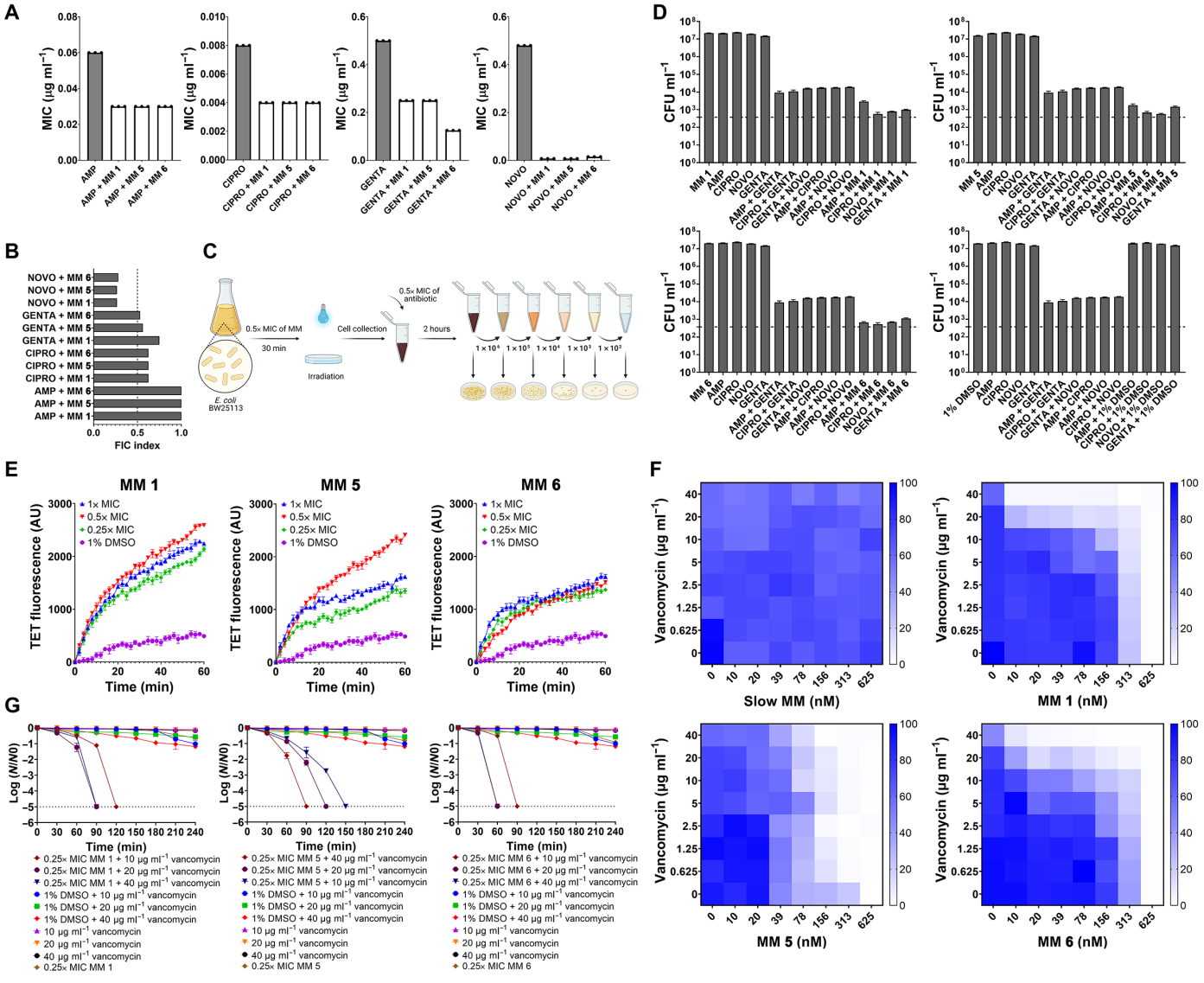

Fig. 6. MMs sensitize bacteria to conventional antibiotics. (**A**) MIC values of different antibiotics in *E. coli* with or without pretreatment with light-activated MMs. (**B**) FIC index for the interaction between MMs and different antibiotics in *E. coli*. (**C**) Workflow used to investigate the ability of MMs to potentiate antibiotic activity created with Biorender.com. (**D**) Reduction in cell numbers following treatment of *E. coli* with 1% DMSO, 0.5× MIC of different MMs, 4× MIC of different antibiotics alone or in combination, or upon challenging 0.5× MIC MM-treated cells with 4× MIC of antibiotics. (**E**) Time-dependent increase in tetracycline fluorescence in *E. coli* following pretreatment of cells with 1% DMSO or MMs. (**F**) Representative checkerboards depicting the interaction between visible light–activated MMs and vancomycin in *P. aeruginosa*. A slow MM (ARV-3-202) was used as a control. Results are shown as a heatmap with the white color denoting no growth (0%) and the blue color denoting growth. Growth was assessed as optical density at 600 nm (OD_{600}). (**G**) Time-kill curves of *P. aeruginosa* treated with 0.25× MIC of the different visible light–activated MMs and subsequently challenged with vancomycin. Vancomycin-only and MM-only treated samples, as well as DMSO controls, were also examined. AMP, ampicillin; CIPRO, ciprofloxacin; GENTA, gentamicin; NOVO, novobiocin. All experiments were conducted at least in triplicate. Where appropriate, results are shown as the mean of at least three biological replicas ± standard error of the mean. Unless otherwise noted, results for MMs and DMSO are always reported in the presence of light.

that pretreatment with MM **1**, MM **5**, and MM **6** resulted in a substantial increase in intracellular tetracycline fluorescence compared to DMSO-treated samples (Fig. 6E) further indicates that MM potentiates antibiotic killing by permeabilizing the cell membrane and facilitating access of antibiotics to their intracellular targets.

The ability of pretreatment with sublethal MM concentrations to potentiate antibiotic action was further investigated in *P. aeruginosa* treated with sub-MIC concentrations of the three most potent MMs (MM **1**, MM **5**, and MM **6**) and then challenged with increasing concentrations of the antibiotic vancomycin. Because of its large size, vancomycin (~1450 Da) usually cannot cross the outer membrane of Gram-negative bacteria (*18*). However, pretreatment with sub-MIC concentrations of MMs resulted in increased susceptibility of *P. aeruginosa* to vancomycin, denoted by inhibition of growth in checkerboard plates (Fig. 6F). Accordingly, *P. aeruginosa* cells pretreated with 0.25× MIC of the different visible light–activated MMs were killed in 60 to 150 min of treatment with vancomycin (Fig. 6G).

Therapeutic doses of MMs mitigate infection-associated mortality in vivo

The toxicity of MMs to mammalian cells was originally investigated by examining the light dose–dependent effects of different concentrations of the most potent MMs (MM **1**, MM **5**, and MM **6**) in human embryonic kidney (HEK) cells. The results revealed a reduction in viability of HEK cells with increasing concentration of MMs and increasing light dose (fig. S14). The safety of MMs was further examined in both HEK cells and normal human dermal fibroblasts (NHDFs) by determining the MM concentration resulting in a 50% reduction in the viability of mammalian cells [median inhibitory concentration (IC_{50})] following 5 min of irradiation at 146 mW cm^{-2} (43.8 J cm^{-2}), the same experimental conditions used to determine the bacterial MIC (table S11). For NHDFs, the IC_{50} ranged from 5 μM for MM **1** to 10 μM for MM **5** and MM **6**. For HEK cells, the IC_{50} was 5 μM for the three MMs tested. On the basis of these results, a concentration of 1× the MIC of each MM (table S3) was used for subsequent in vivo experiments.

The in vivo antibacterial activity of MMs was investigated in a burn wound infection model of the invertebrate *Galleria mellonella* (*19*). Following the generation of a burn wound in the worm, wounds were infected with either the Gram-positive *S. aureus* or the Gram-negative *A. baumannii*. Infected wounds were then treated with 1% DMSO, 1× MIC of conventional antibiotics (polymyxin B in the case of *A. baumannii* infection and tobramycin in the case of *S. aureus* infection), 1% DMSO, or 1× MIC of MM **1**, MM **5**, or MM **6** for each bacterial strain and 43.8 J cm^{-2} of 405-nm light (Fig. 7A). The survival of worms under different treatments was monitored for up to 7 days after treatment.

All (100%) worms infected with *A. baumannii* and treated with 1% DMSO only (no light) died by day 6 after treatment (Fig. 7B). Treatment with 1× MIC of polymyxin B attenuated mortality after 7 days to 69% ($P < 0.0001$; table S12), while treatment with MMs attenuated mortality after 7 days to 40 to 60% ($P < 0.0001$). In the case of worms infected with *S. aureus* and treated with 1% DMSO (no light), 100% mortality was observed 7 days after treatment. Treatment with 1× MIC of tobramycin mitigated mortality at 7 days to 33%, while treatment with MMs mitigated mortality after 7 days to 17 to 25% ($P < 0.0001$).

DISCUSSION

Here, we describe an antibacterial therapy based on the use of synthetic visible light–activated MMs that kill bacteria by mechanical damage. At therapeutic doses, synthetic MMs were activated by visible light to kill Gram-positive and Gram-negative bacteria, including MRSA, within minutes, vastly outperforming conventional antibiotics (Fig. 2, A and B).

Besides exponentially growing cells, MMs also rapidly eliminated persister cells (Fig. 3A). Persister cells are defined as transiently antibiotic-tolerant fractions of bacterial populations that are metabolically inactive or dormant (*20*). In this phenotypic state, the biosynthetic processes targeted by standard antimicrobial therapies are inactive or significantly attenuated, making them highly tolerant to conventional antibiotics that typically affect growing bacteria with an active metabolism (*21*–*23*).

MMs were also able to significantly reduce the cell number and biomass of established biofilms of *P. aeruginosa* and *S. aureus* (Fig. 3, B to E). Similar to persister cells, biofilms are considered resistant phenotypes, characterized by the presence of a heterogeneous dense extracellular polymeric matrix that includes extracellular DNA, proteins, and polysaccharides in which high densities of microbial cells are entrapped (*24*). This complex milieu provides a barrier to antibiotic diffusion and penetration, making biofilm-associated infections frequently refractory to conventional antimicrobial therapy (*25*–*27*). However, the irradiation conditions necessary for complete elimination of biofilms are much higher than those safe for mammalian cells (table S11), and at the extended irradiation times necessary to completely reduce biofilm biomass (up to 45 min), an effect of temperature cannot be excluded. Contrary to conventional antibiotics, repeated exposure to MMs in serial passage experiments (*28*) was not accompanied by a change in MIC value (Fig. 3F), suggesting a low propensity for the development of resistance to MM therapy across different bacteria.

Since MM-resistant mutants could not be isolated, the mechanism of action of these new molecules was investigated using gene expression analysis via RNA-seq, an array of spectrophoto- and spectrofluorimetric methods, and electron microscopy in *E. coli*. MM- and DMSO-treated cells displayed notably distinct transcriptomic profiles (Fig. 4C). Transcripts significantly more abundant in DMSO-treated cells compared to MM-treated cells were overwhelmingly enriched for membrane-associated processes (tables S7 to S9), identifying the membrane as the major target of MMs. Increased fluorescence of dyes used to monitor damage to the inner and outer bacterial membrane (Fig. 5, A and B) further demonstrated that the mechanism of action of MMs involves unspecific, widespread damage to the cell envelope. Membrane damage was followed by leakage of intracellular components, denoted by increased levels of

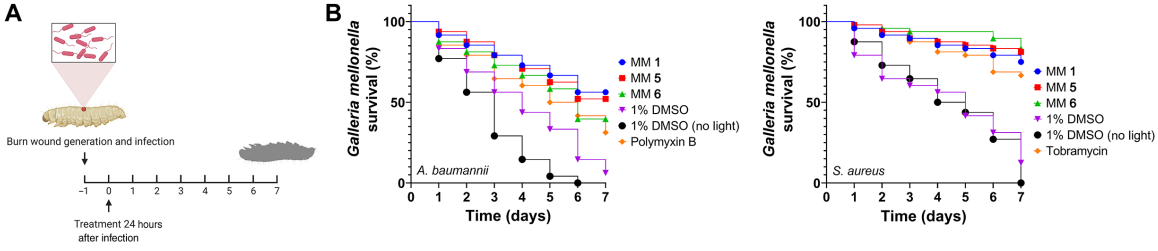

Fig. 7. MMs mitigate mortality in vivo. (**A**) Workflow used to assess the in vivo antibacterial effects of MMs created with Biorender.com. (**B**) Percent survival of *G. mellonella* infected with *A. baumannii* or *S. aureus* and treated with 1× MIC of different MMs, 1% DMSO in the presence or absence of 405-nm light, or the antibiotics polymyxin or tobramycin. Data represent the pooled results from three independent biological replicas, each containing 16 individuals. Unless otherwise noted, results for MMs and DMSO are always reported in the presence of light.

extracellular ATP (Fig. 5C), and loss of the ability to sustain the membrane potential, evidenced by increased fluorescence of the membrane potential dye $DiSC_3(5)$ (Fig. 5D). Electron microscopy revealed extensive damage to the cell ultrastructure following MM treatment, particularly at the level of the membrane and cell wall, including the presence of physical deformities reminiscent of holes in the cell surface that were absent in DMSO controls (Fig. 5, E and F).

These results suggest that the mode of action of MMs is distinct from that of membrane-targeting, pore-forming antibiotics such as nisin or daptomycin, which involve docking to specific binding sites in the membrane and the oligomerization of the antibiotic molecule to form a pore or ion channel (*29*, *30*). Resistance to these antibiotics has been reported and attributed to altered cell wall and cell membrane composition and function in resistant mutants (*31*, *32*). The fact that MMs were able to rapidly kill a range of Gram-positive and Gram-negative bacteria, including antibiotic-resistant strains and efflux knockouts, suggests that the antibacterial action of MMs does not involve binding to specific elements within the bacterial envelope. Rather, the mechano-bactericidal action of MMs via physical membrane disruption is unlike any other antibacterial modality of which we are aware. This molecular-level generalized, unspecific membrane damage can also possibly account for the ability of MMs to efficiently eradicate persisters, which are particularly susceptible to membrane-targeting agents (*33*). Further studies using MMs coupled with fluorescent molecules will be useful in visualizing the precise positioning of the MMs within the cell membrane and whether, once inside the cell, they may bind and destroy other intracellular targets.

A mode of action that involves physical membrane disruption may also explain the undetectable levels of resistance after repeated exposure to MMs (Fig. 3F). A low propensity for resistance development could also be explained by the involvement of two distinct modes of action in the antibacterial activity of MMs: (i) physical membrane damage resulting from fast rotation of MMs following light activation and (ii) antibacterial effects of blue light. Blue light (400 to 490 nm) has well-known antibacterial properties (*34*–*37*) and also shows a low propensity for resistance development (*37*, *38*). The antibacterial mechanism of action of blue light appears to involve the generation of reactive oxygen species (ROS) and subsequent oxidative damage to biomolecules (*39*–*41*). However, under our experimental setup, a significant difference in ROS levels in MM-treated cells and DMSO-treated cells using the ROS-sensitive probes 2′-7′dichlorofluorescin diacetate (DCFH-DA) and aminophenyl fluorescein (APF) was not detected at either the population (microplate format) or single-cell (flow cytometry) levels in the case of MM **1** and MM **6**, while treatment with MM **5** resulted in a small increase in DCFH-DA–positive cells (fig. S15, A to F). Singlet oxygen generation by the irradiated antibacterial motor MM **1**, detected using the singlet oxygen trap 1,3-diphenylisobenzofuran (DPBF) (*11*), was lower than that of its slow, inert counterpart (fig. S15, G to I), suggesting that singlet oxygen generation is not associated with the antibacterial potential of molecular motors. Likewise, the levels of protein carbonyls in cells treated with DMSO or the potent antibacterial motor MM **1** were not significantly changed (fig. S15J). In addition, the MM-induced inactivation profiles of *E. coli* treated with ROS scavengers before irradiation were similar to those of untreated cells (fig. S16). Together, these results indicate that ROS does not play a significant role in MM-induced bacterial killing. ROS quenching by the central twisted carbon-carbon double-bond characteristic of MMs was previously reported (*42*) and, to a certain extent, was also observed in the present study (fig. S15E).

Antibacterial effects were only observed in MM-treated cells that were irradiated but not in those kept in the dark, denoting the importance of light for the antibacterial effects of MMs. Since the irradiation conditions used for most experiments (5 min of irradiation with 405-nm light at 146 mW cm^{-2}) did not result in a significant increase in temperature and the temperature variations in samples treated with fast antibacterial MMs (23.9° ± 1.3°C) and slow MMs (24.4° ± 1.3°C) without antibacterial activity were similar (fig. S17), temperature alone cannot account for the antibacterial effects of MMs. In addition, irradiated MMs maintained their integrity and biological activity and did not undergo photodecomposition, as evidenced by nuclear magnetic resonance (NMR) spectra before and after irradiation, displaying only changes in isomer ratios but the absence of new aromatic signals (fig. S18). Sustained antibacterial activity of extensively preirradiated MMs (fig. S19) further excludes phototoxicity as the mechanism of action of MMs. Last, slow MMs (10^{-3} Hz) chemically analogous to antibacterial MMs (≈3 MHz) did not exhibit antibacterial activity (fig. S3), demonstrating the importance of fast mechanical rotation for the antibacterial properties of MMs.

Together, these results indicate that, under the experimental conditions examined, MM-induced antibacterial effects can be attributed to the rapid drilling-like unidirectional rotation of MMs following light activation, whereby the rotor portion of the molecule spins around the central olefinic bond (Fig. 1B), propelling the molecule through the membrane (Fig. 1C). Subsequent leakage of cell contents and loss of membrane potential eventually culminate in bacterial cell death.

The reduced permeability of the Gram-negative membrane represents an important challenge for antibacterial therapy by posing a barrier that limits antibiotic entrance to the cell (*43*, *44*). In this work, we observed that, besides their direct antibacterial properties, MMs were able to potentiate the killing of *E. coli* by traditional antibiotics, as demonstrated by (i) a reduction of antibiotic MIC values when antibiotic treatment was preceded by exposure of cells to sublethal doses of MMs (Fig. 6A) and (ii) enhanced killing by antibiotics following preexposure of cells to sublethal MMs (Fig. 6D). Increased intracellular tetracycline fluorescent signal in cells pretreated with visible light–activated MMs (Fig. 6E) suggests that the enhanced antibiotic killing of cells pretreated with MMs is a result of MM-induced cell permeabilization and increased accessibility of antibiotics to their intracellular targets.

This effect was observed not only in *E. coli* but also in the opportunistic pathogen *P. aeruginosa*. Because of its hydrophilicity and large size, vancomycin (~1450 Da) usually cannot cross the outer membrane of Gram-negative bacteria (*18*). However, *P. aeruginosa* challenged with sublethal concentrations of fast light-activated MMs displayed substantial growth inhibition following subsequent treatment with vancomycin (Fig. 6F) and were completely killed in as little as 60 min by the otherwise ineffective vancomycin (Fig. 6G). These results demonstrate the ability of MMs to permeabilize the Gram-negative outer membrane to substances that would otherwise be excluded, including typical Gram-positive antibiotics such as vancomycin.

The results obtained in this study demonstrate that, by permeabilizing the Gram-negative outer membrane and improving the accessibility of antibiotics to intracellular targets, MMs exert an antibiotic coadjuvant action. Future work should aim to identify other

antibacterial molecules whose action can be potentiated by visible light–active MM-induced membrane permeabilization.

The safety of MMs to mammalian cells was investigated in vitro in two mammalian cell lines subjected to the same irradiation conditions used to determine the bacterial MIC. The intensity (146 mW cm^{-2}) and dose/fluence (43.8 J cm^{-2}) of 405-nm light used throughout most of this study are comparable, or lower, to those previously shown to be safe for mammalian cells in vitro and in vivo (*40*, *45*–*48*). The proximity of the IC_{50} and MIC (table S11), particularly in *A. baumannii*, demonstrates the broad destructive capabilities of MMs, previously reported for UV-activated MMs (*11*, *49*).

Given these safety concerns, the invertebrate infection model *G. mellonella* was used to investigate the in vivo anti-infective capabilities of MMs. *G. mellonella* is a well-established, inexpensive, and low maintenance model of fungal and bacterial infections (*50*–*53*). While insects such as *G. mellonella* do not have an adaptive immune response and cannot generate antibodies, their complex innate immune system shows some similarities to that of mammals (*54*). Correlations between immune responses to pathogens in *G. mellonella* and mice demonstrate that results obtained using this invertebrate model can provide significant insights into the mammalian response (*55*–*57*).

Because of their location, skin wounds, such as burns, are particularly amenable to light-mediated antimicrobial therapies. Systemic antimicrobials have limited efficiency in the treatment of these localized infections due to poor blood flow to these areas and the presence of dead tissue (*58*, *59*) while potentially contributing to the development of resistance in nontarget organisms (*59*). A *G. mellonella* burn wound infection model was recently described (*19*).

In this work, burn wounds of *G. mellonella* were infected with two of the major bacterial pathogens typically associated with burn wounds, *A. baumannii* and *S. aureus* (*60*, *61*). Treatment of infected worms with visible light–activated MMs mitigated the mortality associated with infection by both *A. baumannii* and *S. aureus* (Fig. 7B). Mortality mitigation by MMs (up to 83%) was similar or superior to that of conventional antibiotics. These results demonstrate the potential of MMs in the treatment of localized bacterial infections, despite the small therapeutic window.

Future next-generation MMs need to not only be potent antibacterials but also display improved selectivity toward bacteria with minimal damage to mammalian cells, for instance, by increasing the number of positive charges within MMs to enhance their affinity toward the negatively charged bacterial membrane but not the more neutrally charged mammalian membrane (*62*). Bacteria-specific peptide addends (*63*) linked to either the stator or the rotor portion of the molecule can also be used for the targeted killing of bacteria by MMs. Alternatively, safe and effective antibacterial effects can be achieved by combining light-activated MMs and conventional antibiotics, whereby bactericidal action can be exerted at sublethal MM concentrations, circumventing potential MM toxicity.

MATERIALS AND METHODS

Synthetic chemistry

Details on the synthesis and characterization of the MMs used in this study are provided in the Supplementary Materials.

Preparation of cells for irradiation experiments

Cells from glycerol stocks maintained at −80°C were streaked onto LB agar plates to get single isolated colonies. One single colony was picked up from the plate and grown overnight in 5 ml of filter-sterilized LB medium in a 50-ml falcon tube (220 rpm at 30° or 37°C depending on the strain). The following day, 1 ml of the overnight culture was added to 50 ml of filter-sterilized LB medium in a 250-ml Erlenmeyer flask and incubated until an optical density at 600 nm (OD_{600}) of approximately 1. A volume of 500 µl of this culture was diluted into 50 ml of fresh filter-sterilized LB medium and centrifuged for 15 min at 5000 rpm, 25°C. Afterward, the pellet was resuspended in phosphate-buffered saline (PBS) to a final OD_{600} of ≈0.05.

Irradiation experiments

The appropriate volume of an MM stock at 8 mM necessary to achieve a concentration ranging from 0.3125 to 40 µM was pipetted into a 2-ml microcentrifuge tube to which 1 ml of cell suspension prepared as previously described was added. Corresponding negative controls (DMSO only) were prepared in the same way. The mixture was gently mixed by pipetting and incubated in the dark at 30° or 37°C, depending on the strain, for 30 min with agitation (220 rpm). Afterward, MM- or DMSO-treated cells were dispensed in one well of a 24-well plate positioned in the center of the light beam (405-nm light-emitting diode light, UHP-F-5-405, Prizmatix, Israel) placed at the appropriate distance necessary to achieve the desired light intensity of 304, 146, or 87 mW cm^{-2}, as measured using a handheld digital power meter console coupled to an S415C thermal power sensor head (Thorlabs, Newton, MA, USA). The temperature during irradiation was monitored using a thermocouple probe (model SC-TT-K-30-36-PP, Omega Engineering Inc., Stanford, CT, USA). Samples were agitated during irradiation. Dark controls were prepared as previously described except that no irradiation was provided.

Minimum inhibitory concentration

For MIC determination, samples were treated with a range of concentrations of the different MMs as described above and were irradiated one at a time for 5 min at 146 mW cm^{-2} (43.8 J cm^{-2}), after which irradiated aliquots were collected and inoculated into 1 ml of MHB in a 2-ml microcentrifuge tube. Samples were incubated overnight at 30° or 37°C, depending on the strain, without agitation. Corresponding nonirradiated samples and negative controls (without bacteria) were also included. The following day, cultures were inspected for growth, and the MIC was identified. The experimental procedure used to determine the MIC of visible light–activated MMs is schematically depicted in fig. S2.

Time-kill experiments

For time-kill experiments, 50-µl aliquots in triplicate of samples treated with 2× MIC determined as described above were collected at different time points (0, 1, 2, 3, 4, 5, 10, and 15 min) following 405-nm irradiation at different light intensities (87, 146, and 304 mW cm^{-2}, corresponding to a distance between sample and light source of 20, 15, and 10 cm, respectively). For light dose–dependent experiments, samples were exposed to different concentrations of the most potent MMs (MM **1**, MM **5,** and MM **6**) and irradiated with 0, 1, 2, 4, 8, 16, 32, 40, and 80 J cm^{-2}. Serial dilutions of irradiated cell suspensions were prepared in PBS. A volume of 10 µl of the appropriate serial dilutions was spot-plated onto LB agar plates. Following overnight incubation at 30° or 37°C, depending on the strain, bacterial viability was assessed as colony-forming units (CFUs) per milliliter. Results were expressed as log ($N/N0$), whereby N is the CFU per milliliter at each irradiation time point and $N0$ is the initial CFU per milliliter of the

corresponding sample. Only dilutions that yielded 10 to 100 colonies were counted.

Preparation and eradication of persister and persister-like cells

Persisters of *A. baumannii* and *P. aeruginosa* were generated by growing cell cultures to late-stationary phase for 16 hours at 37°C, followed by treatment with ciprofloxacin (10-fold MIC) for 4 hours to kill nonpersistent cells (*64*). Persister cells of *E. coli* were prepared by adding ampicillin (100 μg ml^{-1}) to exponential-phase cells (OD_{600} of ≈0.8), followed by continuous agitation for another 3 hours, as previously described (*14*). In the case of *S. aureus*, almost all stationary phase cells are considered to be persistent (*14*). *S. aureus* cells were grown at 37°C and 220 rpm in LB broth to an OD_{600} of 0.3. Cells were then diluted 1:1000 in 25 ml of LB and grown for 16 hours at 37°C and 220 rpm in 250-ml flasks. Antibiotic-tolerant or stationary phase persister cells of Gram negatives and *S. aureus*, respectively, were collected and resuspended in PBS and then challenged with 1× MIC of MMs or 1% DMSO, followed by irradiation at 405 nm at a dose of 146 mW cm^{-2}, as described for exponential phase cells. Antibiotic controls (2× and 4× MIC) were processed in the same way, except that no light was provided. At specified time points (0, 1, 2, 3, 4, 5, 10, and 15 min), 50-μl aliquots were removed, serially diluted, and spot-plated onto LB agar plates to determine CFU per milliliter. Only dilutions that yielded 10 to 100 colonies were counted. Results were expressed as log (*N*/*N*0), whereby *N* is the CFU per milliliter at each irradiation time point, and *N*0 is the initial CFU per milliliter of the corresponding sample. Only dilutions that yielded 10 to 100 colonies were counted.

Antibiofilm potential of visible light–activated MMs

The antibiofilm potential of the most potent MMs (MM **1**, MM **5**, and MM **6**) was assessed in a 96-well plate format using a combination of methods targeting different components of the biofilm (*15*): Acridine orange was used to quantify the total bacteria cell number, ATP levels were used to quantify metabolically active cells within the biofilm, crystal violet was used to quantify biofilm biomass, and fluorescein isothiocyanate (FITC) was used to quantify total protein in the biofilm matrix. This combination of methods is effective at evaluating the antibiofilm potential of chemicals (*15*). *P. aeruginosa* and *S. aureus* were grown overnight in tryptic soy broth (TSB) medium. The overnight cultures were diluted in 1:100 in fresh medium, and 100-μl aliquots were distributed in a 96-well plate. After 24 hours of static growth at 37°C, planktonic cells were removed by inverting the plate onto a stack of paper towels, and the biofilm was washed three times with PBS. After washing, MM **1**, MM **5**, or MM **6** was added at 2× MIC to the biofilm and incubated statically in the dark for 60 min. The biofilm was then irradiated for 15, 30, or 45 min at 146 mW cm^{-2}. For the determination of the total bacterial number, acridine orange solution (2% w/v in H_2O) diluted 1:100 in Walpole's buffer (27.2 g $liter^{-1}$ of sodium acetate trihydrate, adjusted to pH 4 with glacial acetic acid) was added to the wells. Following a 15-min incubation, the biofilm was washed three times with 0.9% NaCl, thoroughly resuspended in 100 μl of 0.9% NaCl, and fluorescence intensity (excitation, 485 nm; emission, 528 nm) was measured in a microplate reader (BioTek Instruments Inc., Winooski, VT, USA) (*15*).

For quantification of viable cells in biofilms, following the addition of 100 μl of TSB to each well, bacteria were detached from the biofilm by thorough mixing, after which 100 μl of BacTiter-Glo reagent (BacTiter-Glo Microbial Cell Viability Assay, Promega, WI, USA), prepared according to the manufacturer's instructions, was added to each well. After a 5-min incubation, the luminescence intensity was measured in a microplate reader (BioTek Instruments Inc., Winooski, VT, USA) (*15*).

For total biofilm protein quantification, 250 μl of FITC solution (20 μg ml^{-1}) was added to each well. Following a 30-min incubation, the biofilm was thoroughly washed with 0.9% NaCl and then resuspended in 100 μl double-distilled H_2O. Fluorescence intensity was measured (excitation, 485 nm; emission, 528 nm) in a microplate reader (BioTek Instruments Inc., Winooski, VT, USA) (*15*).

For total biofilm biomass quantification, 100 μl of TSB medium was added to the irradiated biofilm. Following 24 hours of recovery at 37°C, plates were again inverted onto a stack of paper towels, and the biofilm was then washed with water by submersion of the plate. The washed biofilm was stained with a 0.1% solution of crystal violet in water. After 15 min of staining, the plate was rinsed three times with water and then blotted on a stack of paper towels. After overnight drying of the plate, 30% acetic acid in water was added to solubilize the crystal violet for 15 min. The solubilized crystal violet was transferred to a new flat-bottom microtiter plate, and the absorbance at 550 nm was quantified in a microplate reader (BioTek Instruments Inc., Winooski, VT, USA) using 30% acetic acid in water as the blank (*65*). Unirradiated samples were used as controls. Control antibiotics rifampin (*P. aeruginosa*) and tobramycin (*S. aureus*) at 2× MIC were also included and processed as described for MMs.

Resistance development

Isolation of MM-resistant mutants of *E. coli*, *A. baumannii*, *P. aeruginosa*, and *S. aureus* was attempted by irradiating cell suspensions treated with 4× MIC of the different MMs for 5 min at 146 mW cm^{-2} (43.8 J cm^{-2}). No visible colonies could be obtained for any of the strains tested.

For resistance development by sequential passaging (*66*), *A. baumannii*, *E. coli*, *P. aeruginosa*, and *S. aureus* cells in exponential phase were collected and processed as described for MIC determination. Cells were incubated at 37°C for 24 hours after which they were inspected for growth. Cells able to grow at 0.5× MIC were collected and rechallenged with a range of MM concentrations and then irradiated. The antibiotics ciprofloxacin and gentamicin (for Gram negatives) or ciprofloxacin and tobramycin (for *S. aureus*) were used as controls.

RNA sequencing

Three independent, well-isolated colonies of *E. coli* were cultured to mid-log phase in MHB medium. Cells were collected and resuspended in PBS (1×) to an OD_{600} of ≈0.05. Cells were treated with 0.5× MIC of MM **1** or 1% DMSO in the dark for 30 min. Cells were then irradiated for 5 min at 146 mW cm^{-2} (43.8 J cm^{-2}). Bacterial cells were collected onto a 0.2-μm polyethersulfone (PES) filter by low-vacuum filtration. Two volumes of RNAprotect (QIAGEN, Valencia, CA) were added to the cells, and the samples were then centrifuged at 5000*g* for 25 min at 4°C to pellet cells. RNA was isolated using the RNeasy Mini Kit (QIAGEN, Valencia, CA) per the manufacturer's instructions. RNA-seq and data analysis were performed by DNA Link Inc. (Seoul, Republic of Korea). RNA-seq libraries were constructed using TruSeq Stranded Total RNA with Ribo-Zero Plus rRNA Depletion Kit and sequenced on the Illumina

NovaSeq6000 platform (Illumina, San Diego, CA) in the 100-nt, paired-end configuration. From each sample, an average of 70 million reads was obtained. For gene expression analysis, reads were trimmed with cutadapt (*67*) and aligned to the reference genome of *E. coli* str. K-12 substr. MG1655 (NC_000913) using EDGE-pro pipeline with default setting. Differential expression analysis was performed with DESeq2 in Bioconductor (*68*). Gene annotation was performed using an in-house script based on National Center for Biotechnology Information reference annotations.

GO enrichment analysis of the transcripts displaying significant differences ($P < 0.05$) in abundance between MM- and DMSO-treated cells was performed using Panther (http://pantherdb.org/) using the Fisher's exact test. Results were corrected for the false discovery rate.

Outer membrane permeability

The impact of treatment with MMs on the outer membrane permeability of *E. coli* was determined using the NPN uptake assay as previously described (*16*). The pore-forming antibiotic nisin was used as a positive control for membrane damage. Cells were washed and resuspended in buffer [5 mM Hepes and 5 mM glucose (pH 7.4)] and treated with different concentrations of MM **1**, MM **5**, and MM **6**, or 1% DMSO. Following irradiation as described for MIC determination, 100 μl of the bacteria suspension was mixed with NPN (final concentration of 2 μg ml^{-1}) in a 96-well black plate. NPN fluorescence was then monitored (excitation, 350 nm; emission, 420 nm) as a function of time using a microplate reader (BioTek Instruments Inc., Winooski, VT, USA). Results were expressed as relative fluorescent units (RFU) corrected for fluorescence in the absence of NPN and in the absence of cells.

Inner membrane permeability

E. coli cells were prepared as previously described and treated with a range of concentrations of MM **1**, MM **5**, and MM **6** and irradiated with 405-nm light at an intensity of 146 mW cm^{-2}. Nisin was used as a positive control. Following irradiation, PI was added to the cells at a final concentration of 2 μg ml^{-1} (*69*). After 30 min of incubation, 200 μl of bacterial suspension was added into a black 96-well plate, and the time-dependent progression of fluorescence intensity (excitation, 535 nm; emission, 620 nm) was recorded in a microplate reader (BioTek Instruments Inc., Winooski, VT, USA). Results were expressed RFU corrected for fluorescence in the absence of cells and in the absence of PI.

Cytoplasmic membrane depolarization

The depolarization of the cytoplasmic membrane of *E. coli* by MMs was assessed using the membrane potential-sensitive cyanine dye $DiSC_3(5)$ (*70*). Briefly, exponential phase bacteria were collected, washed and resuspended 5 mM Hepes buffer containing 20 mM glucose (pH 7.2) to an OD of 0.05. This cell suspension was incubated with 100 mM KCl (to equilibrate cytoplasmic and external K^+ concentration) and 0.4 μM $DiSC_3(5)$ until stabilization of the fluorescent signal. Cells were then incubated with different concentrations of MMs and irradiated as described for MIC determination. Carbonyl cyanide 3-chlorophenylhydrazone (CCCP) was used as a positive control (*71*). Cells were then transferred to a black 96-well plate, and the fluorescent signal was monitored (excitation, 622 nm; emission, 670 nm) using a microplate reader (BioTek Instruments Inc., Winooski, VT, USA). Results were expressed as RFU corrected for fluorescence in the absence of $DiSC_3(5)$ and in the absence of cells.

Extracellular ATP

Intracellular content leakage following treatment with MMs was determined by quantifying extracellular ATP (*72*). Following irradiation in the presence of different concentrations of MM **1**, MM **5**, and MM **6**, or 1% DMSO, *E. coli* cells were centrifuged at 13,000*g* for 5 min. Supernatants were recovered and stored at −20°C for ATP analysis. ATP analysis was conducted using the luminescence-based BacTiter-Glo assay (Promega, WI, USA) per the manufacturer's instructions. Nisin was used as a positive control. The levels of ATP in supernatants were derived via a standard curve of ATP standards from 1 nM to 1 μM. Luminescence measurements of ATP standards and culture supernatants were measured in triplicate on a microplate reader (BioTek Instruments Inc., Winooski, VT, USA). Results were expressed as relative light units corrected for fluorescence in the absence of cells.

Electron microscopy

E. coli was cultured to mid-log phase in MHB medium. Cells were collected and resuspended in PBS (1×) to an OD_{600} of ≈0.05. Cells were treated with 0.5× MIC of MM **1** or 1% DMSO in the dark for 30 min. Cells were then irradiated for 5 min at 146 mW cm^{-2} (43.8 J cm^{-2}) after which cells were fixed with Karnovsky's fixative (*73*), postfixed with 1% osmium, and dehydrated with a series of ethanol washes. For TEM, samples were embedded in epoxy resin (PolyBed 812, Polysciences Inc., Warrington, PA, USA) after dehydration in a graded 50 to 100% ethanol concentration series of washes. Ultrathin sections (65 nm) were cut using a Leica EM UC7 ultramicrotome (Leica Microsystems, Wetzlar, Germany) and post-stained with uranyl acetate and lead citrate. Specimens were observed using a JEOL JEM2100 TEM (Hitachi Corporation, Japan) operating at an accelerating voltage of 80 kV. For SEM, following ethanol dehydration, samples were critical point–dried using a Leica EM CPD300 (Leica Microsystems, Wetzlar, Germany), sputter-coated with 10 nm of gold, and imaged with an FEI Apreo SEM (FEI Apreo, Thermo Fisher Scientific, Waltham, MA, USA) using a secondary electron detector.

Interaction with antibiotics

To evaluate synergy between conventional antibiotics and MMs in *E. coli*, the FIC index (*17*) was determined using a modified checkerboard microtiter test in an eight well–by–eight well configuration. Briefly, *E. coli* cell suspensions were prepared as described for MIC determination and treated with an increasing concentration (0.1 to 40 μM) of the different MMs, followed by irradiation for 5 min at 146 mW cm^{-2}. The irradiated cell suspensions were collected and distributed along the *x* axis of a 96-well plate according to a gradient of increasing concentration, followed by the addition of a gradient of increasing concentration of antibiotic (0.00125 to 1 μg ml^{-1}) along the *y* axis of the plate to the irradiated cells. MHB was then added to each well of the plate, and the plate was incubated at 37°C with shaking at 220 rpm for 18 hours under aerobic conditions. Bacterial growth was assessed by measuring the OD_{600} in a microplate reader (BioTek Instruments Inc., Winooski, VT, USA). The FIC was calculated by dividing the MIC of each antibiotic/MM when used in combination by that of the antibiotic/MM alone. The FIC index, obtained by adding both FICs, was

interpreted as indicating a synergistic effect if it was ≤0.5, as additive or indifferent if it was >0.5 and ≤2.0, and as antagonistic if it was >2.0 (*17*).

To evaluate the ability of pretreatment with subinhibitory concentrations of MMs to potentiate killing by antibiotics, *E. coli* were prepared as described for MIC determination and treated with 0.5× MIC of each MM (MM **1**, MM **5**, and MM **6**) or 1% DMSO, followed by 5-min irradiation at 146 mW cm^{-2}. Irradiated cell suspensions were then collected and challenged with 4× MIC of the antibiotics gentamicin, novobiocin, ciprofloxacin, and ampicillin. Following preparation of the appropriate serial dilutions, samples were spot-plated onto LB agar plates, and the number of CFU per milliliter was determined. Nonirradiated, antibiotic-treated (4× MIC) cell suspensions were similarly processed.

To evaluate the ability of pretreatment with MMs to potentiate killing by vancomycin, *P. aeruginosa* cell suspensions were prepared as described for the MIC assessment and treated with a range of concentrations (0 to 1× MIC) of the different antibacterial MMs (MM **1**, MM **5,** and MM **6**) and irradiated for 5 min with 146 mW cm^{-2} of 405-nm light. Following irradiation, cells were collected and distributed along the *x* axis of a 96-well plate according to a gradient of increasing concentration, after which vancomycin was added according to a gradient of increasing concentration (0 to 40 μg ml^{-1}) along the *y* axis of the plate to the irradiated cells. MHB was then added to each well of the plate, and the plate was incubated at 37°C with shaking at 220 rpm for 18 hours under aerobic conditions. Bacterial growth was assessed by measuring the OD_{600} in a microplate reader (BioTek Instruments Inc., Winooski, VT, USA). For time-kill experiments, *P. aeruginosa* cell suspensions prepared as previously described were treated with 0.25× MIC of the different MMs (MM **1**, MM **5**, and MM **6**) and irradiated for 5 min with 146 mW cm^{-2} of 405-nm light. Vancomycin was then added (final concentration of 10, 20, and 40 μg ml^{-1}), and survival (CFU per milliliter) was monitored every 30 min for 4 hours (240 min), as previously described. Controls treated with vancomycin only, MM only, and DMSO plus vancomycin were also included.

Tetracycline uptake

The ability of pretreatment with subinhibitory concentrations of MMs to potentiate antibiotic killing was further evaluated by monitoring the fluorescence of tetracycline. *E. coli* were prepared as described for MIC determination and treated with 0.5× MIC of each MM (MM **1**, MM **5**, and MM **6**) or 1% DMSO, followed by 5-min irradiation at 146 mW cm^{-2}. Irradiated cell suspensions were then collected, and tetracycline (final concentration of 128 μg ml^{-1}) was added. A volume of 100 μl per well of tetracycline-amended cell suspension was transferred to a black 96-well plate, and fluorescence was read every 5 min for 60 min at room temperature in a microplate reader (excitation, 405 nm; emission, 535 nm) (BioTek Instruments Inc., Winooski, VT, USA). Results were expressed as RFU corrected for fluorescence in the absence of cells.

Toxicity profiling and therapeutic index calculation

Biocompatibility of MMs with primary NHDF and HEK293T cells was assessed using the CellTiter-Glo Luminescent Cell Viability Assay (Promega, WI, USA), per the manufacturer's instructions. The MM concentrations that reduced cell viability by 50% (IC_{50}) were identified, and the therapeutic index was calculated as the ratio between the IC_{50} and the MIC at a light intensity of 146 mW cm^{-2}. For light dose–dependent experiments, HEK cells were treated with different concentrations of the most potent MMs (MM **1**, MM **5**, and MM **6**) and irradiated with 0, 1, 2, 4, 8, 16, 32, 40, and 80 J cm^{-2}.

Animal infection model

Animal studies were conducted in the burn wound model *G. mellonella* recently described (*19*). Larvae were purchased from a commercial source at a stage in their life cycle where they do not need to be fed. Larvae were sorted into petri dishes lined with Whatman filter paper (Thermo Fisher Scientific, Pittsburg, PA, USA) and stored at 4°C until use. The larval bodies were sterilized with 70% ethanol. The burn was generated using a soldering iron (Weller WE1010 ESD-Safe Digital 70-Watt Soldering Station, 120 V, Weller Company, Easton, PA, USA) to achieve a consistent burn area of ≈2 mm^2 in the middle section of the back of larvae. This location was chosen, so the wound could be easily visualized without having to physically manipulate the larvae. Immediately after burn, the wound was inoculated with 10 μl of 1:10 dilution of an overnight culture of *A. baumannii* or *S. aureus*. Any larva that showed distress or leakage of hemolymph after the burn process was immediately euthanized by incubating at −20°C for 20 min to minimize suffering. Following overnight incubation at 37°C for the establishment of infection, 10 μl of (i) different MMs at 1× MIC, (ii) antibiotics polymyxin B in the case of *A. baumannii* or tobramycin in the case of *S. aureus*, or (iii) 1% DMSO were applied to the wound. Following a 30-min incubation period in the dark, larvae were physically restrained, covered with an opaque material, leaving only the wound exposed, and then irradiated for 5 min with 146 mW cm^{-2} of 405-nm light (43.8 J cm^{-2}). To minimize any potential temperature effects, a constant flow of 0.2-μm pore size–filtered air was provided to the surface of the worm. Dark 1% DMSO controls were also included. The mortality of larvae after treatment was monitored for up to 7 days. Mortality was recorded by complete melanization of the larval body and complete loss of motility. A brief overview of the protocol is schematically depicted in Fig. 7A. Work in *G. mellonella* was reviewed and approved by the Office of Sponsored Projects and Research Compliance of Rice University.

Statistical analysis

Unless otherwise mentioned, the arithmetic mean and the standard error of the mean across multiple biological and technical replicas were used as the measures of center and spread. The number of replicates for each experiment type are included in the respective figure legends, where appropriate. Unless otherwise noted, all statistical analyses were performed using GraphPad Prism 8.0 (San Diego, CA, USA). When appropriate, data were min-max–normalized. Depending on the sample size, data normality was assessed using an Anderson-Darling normality test, D'Agostino-Pearson omnibus normality test, Shapiro-Wilk normality test, or Kolmogorov-Smirnov normality test with Dallal-Wilkinson-Lilliefor's test for *P* value. Comparisons between two groups were conducted using a *t* test for parametric data or a Mann-Whitney *U* test for nonparametric data. Multiple group comparisons were performed using analysis of variance (ANOVA) or a Kruskal-Wallis test with Dunn's multiple comparisons test. A Mantel-Cox test was used to determine the statistical significance in *G. mellonella* survival assays. A value of $P < 0.05$ was considered statistically significant. Where appropriate, asterisks are used to denote the significance of

differences. *$P < 0.05$, **$P < 0.01$, ***$P < 0.001$, ****$P < 0.0001$. Unless otherwise noted, all figures were generated in GraphPad Prism 8.0 (San Diego, CA, USA).

SUPPLEMENTARY MATERIALS

Supplementary material for this article is available at https://science.org/doi/10.1126/sciadv.abm2055

View/request a protocol for this paper from *Bio-protocol*.

REFERENCES AND NOTES

1. CDC, in *Antibiotic resistance threats in the United States* (U.S. Department of Health and Human Services Centers for Disease Control and Prevention, 2019), pp. 1–113.
2. J. O'Neill, *Review on Antimicrobial Resistance: Tackling Drug-Resistant Infections Globally—Final Report and Recommendations* (Wellcome Trust, U.K. government, 2016).
3. WHO, "No time to wait: Securing the future from drug-resistant infections" (World Health Organization, 2019); https://who.int/docs/default-source/documents/no-time-to-wait-securing-the-future-from-drug-resistant-infections-en.pdf.
4. M. S. Butler, D. L. Paterson, Antibiotics in the clinical pipeline in October 2019. *J. Antibiot.* **73**, 329–364 (2020).
5. Pew Research Center, "Antibiotics currently in global clinical development" (Pew Charitable Trusts, 2020); https://pewtrusts.org/-/media/assets/2017/05/antibiotics-currently-in-clinical-development-03-2017.pdf.
6. J. M. V. Makabenta, A. Nabawy, C.-H. Li, S. Schmidt-Malan, R. Patel, V. M. Rotello, Nanomaterial-based therapeutics for antibiotic-resistant bacterial infections. *Nat. Rev. Microbiol.* **19**, 23–36 (2021).
7. D. P. Linklater, V. A. Baulin, S. Juodkazis, R. J. Crawford, P. Stoodley, E. P. Ivanova, Mechano-bactericidal actions of nanostructured surfaces. *Nat. Rev. Microbiol.* **19**, 8–22 (2021).
8. S. Cheeseman, A. J. Christofferson, R. Kariuki, D. Cozzolino, T. Daeneke, R. J. Crawford, V. K. Truong, J. Chapman, A. Elbourne, Antimicrobial metal nanomaterials: From passive to stimuli-activated applications. *Adv. Sci.* **7**, 1902913 (2020).
9. B. L. Feringa, The art of building small: From molecular switches to molecular motors. *J. Org. Chem.* **72**, 6635–6652 (2007).
10. M. Klok, N. Boyle, M. T. Pryce, A. Meetsma, W. R. Browne, B. L. Feringa, MHz unidirectional rotation of molecular rotary motors. *J. Am. Chem. Soc.* **130**, 10484–10485 (2008).
11. V. García-López, F. Chen, L. G. Nilewski, G. Duret, A. Aliyan, A. B. Kolomeisky, J. T. Robinson, G. Wang, R. Pal, J. M. Tour, Molecular machines open cell membranes. *Nature* **548**, 567–572 (2017).
12. T. Galbadage, D. Liu, L. B. Alemany, R. Pal, J. M. Tour, R. S. Gunasekera, J. D. Cirillo, Molecular nanomachines disrupt bacterial cell wall, increasing sensitivity of extensively drug-resistant *Klebsiella pneumoniae* to meropenem. *ACS Nano* **13**, 14377–14387 (2019).
13. S. Roy, Impact of UV radiation on genome stability and human health, in *Ultraviolet Light in Human Health, Diseases and Environment*, S. I. Ahmad, Ed. (Springer, 2017), pp. 207–219.
14. I. Keren, N. Kaldalu, A. Spoering, Y. Wang, K. Lewis, Persister cells and tolerance to antimicrobials. *FEMS Microbiol. Lett.* **230**, 13–18 (2004).
15. P. Stiefel, U. Rosenberg, J. Schneider, S. Mauerhofer, K. Maniura-Weber, Q. Ren, Is biofilm removal properly assessed? Comparison of different quantification methods in a 96-well plate system. *Appl. Microbiol. Biotechnol.* **100**, 4135–4145 (2016).
16. I. M. Helander, T. Mattila-Sandholm, Fluorometric assessment of Gram-negative bacterial permeabilization. *J. Appl. Microbiol.* **88**, 213–219 (2000).
17. M. J. Hall, R. F. Middleton, D. Westmacott, The fractional inhibitory concentration (FIC) index as a measure of synergy. *J. Antimicrob. Chemother.* **11**, 427–433 (1983).
18. E. Rubinstein, Y. Keynan, Vancomycin revisited–60 years later. *Front. Public Health* **2**, 217 (2014).
19. E. Maslova, Y. Shi, F. Sjöberg, H. S. Azevedo, D. W. Wareham, R. R. McCarthy, An invertebrate burn wound model that recapitulates the hallmarks of burn trauma and infection seen in mammalian models. *Front. Microbiol.* **11**, 998 (2020).
20. K. Lewis, Persister cells, dormancy and infectious disease. *Nat. Rev. Microbiol.* **5**, 48–56 (2007).
21. K. Lewis, Persister cells. *Annu. Rev. Microbiol.* **64**, 357–372 (2010).
22. K. R. Allison, M. P. Brynildsen, J. J. Collins, Metabolite-enabled eradication of bacterial persisters by aminoglycosides. *Nature* **473**, 216–220 (2011).
23. B. P. Conlon, E. S. Nakayasu, L. E. Fleck, M. D. LaFleur, V. M. Isabella, K. Coleman, S. N. Leonard, R. D. Smith, J. N. Adkins, K. Lewis, Activated ClpP kills persisters and eradicates a chronic biofilm infection. *Nature* **503**, 365–370 (2013).
24. J.-H. Ch'ng, K. K. L. Chong, L. N. Lam, J. J. Wong, K. A. Kline, Biofilm-associated infection by enterococci. *Nat. Rev. Microbiol.* **17**, 82–94 (2019).
25. P. S. Stewart, Mechanisms of antibiotic resistance in bacterial biofilms. *Int. J. Med. Microbiol.* **292**, 107–113 (2002).
26. C. Vuotto, F. Longo, M. P. Balice, G. Donelli, P. E. Varaldo, Antibiotic resistance related to biofilm formation in *Klebsiella pneumoniae*. *Pathogens* **3**, 743–758 (2014).
27. R. M. Donlan, Role of biofilms in antimicrobial resistance. *ASAIO J.* **46**, S47–S52 (2000).
28. M. O. A. Sommer, C. Munck, R. V. Toft-Kehler, D. I. Andersson, Prediction of antibiotic resistance: Time for a new preclinical paradigm? *Nat. Rev. Microbiol.* **15**, 689–696 (2017).
29. C. Kosmidis, D. P. Levine, Daptomycin: Pharmacology and clinical use. *Expert Opin. Pharmacother.* **11**, 615–625 (2010).
30. A. Prince, P. Sandhu, P. Ror, E. Dash, S. Sharma, M. Arakha, S. Jha, Y. Akhter, M. Saleem, Lipid-II independent antimicrobial mechanism of nisin depends on its crowding and degree of oligomerization. *Sci. Rep.* **6**, 37908 (2016).
31. T. T. Tran, J. M. Munita, C. A. Arias, Mechanisms of drug resistance: Daptomycin resistance. *Ann. N. Y. Acad. Sci.* **1354**, 32–53 (2015).
32. A. S. Bayer, T. Schneider, H.-G. Sahl, Mechanisms of daptomycin resistance in *Staphylococcus aureus*: Role of the cell membrane and cell wall. *Ann. N. Y. Acad. Sci.* **1277**, 139–158 (2013).
33. J. G. Hurdle, A. J. O'Neill, I. Chopra, R. E. Lee, Targeting bacterial membrane function: An underexploited mechanism for treating persistent infections. *Nat. Rev. Microbiol.* **9**, 62–75 (2011).
34. M. R. Hamblin, J. Viveiros, C. Yang, A. Ahmadi, R. A. Ganz, M. J. Tolkoff, *Helicobacter pylori* accumulates photoactive porphyrins and is killed by visible light. *Antimicrob. Agents Chemother.* **49**, 2822–2827 (2005).
35. T. Dai, A. Gupta, C. K. Murray, M. S. Vrahas, G. P. Tegos, M. R. Hamblin, Blue light for infectious diseases: *Propionibacterium acnes*, *Helicobacter pylori*, and beyond? *Drug Resist. Updat.* **15**, 223–236 (2012).
36. Y. Wang, X. Wu, J. Chen, R. Amin, M. Lu, B. Bhayana, J. Zhao, C. K. Murray, M. R. Hamblin, D. C. Hooper, T. Dai, Antimicrobial blue light inactivation of gram-negative pathogens in biofilms: *In vitro* and *in vivo* studies. *J Infect Dis* **213**, 1380–1387 (2016).
37. R. M. Amin, B. Bhayana, M. R. Hamblin, T. Dai, Antimicrobial blue light inactivation of *Pseudomonas aeruginosa* by photo-excitation of endogenous porphyrins: *In vitro* and *in vivo* studies. *Lasers Surg. Med.* **48**, 562–568 (2016).
38. Y. Zhang, Y. Zhu, J. Chen, Y. Wang, M. E. Sherwood, C. K. Murray, M. S. Vrahas, D. C. Hooper, M. R. Hamblin, T. Dai, Antimicrobial blue light inactivation of *Candida albicans*: *In vitro* and *in vivo* studies. *Virulence* **7**, 536–545 (2016).
39. F. Cieplik, A. Späth, C. Leibl, A. Gollmer, J. Regensburger, L. Tabenski, K.-A. Hiller, T. Maisch, G. Schmalz, Blue light kills *Aggregatibacter actinomycetemcomitans* due to its endogenous photosensitizers. *Clin. Oral Investig.* **18**, 1763–1769 (2014).
40. T. Dai, A. Gupta, Y.-Y. Huang, R. Yin, C. K. Murray, M. S. Vrahas, M. E. Sherwood, G. P. Tegos, M. R. Hamblin, Blue light rescues mice from potentially fatal *Pseudomonas aeruginosa* burn infection: Efficacy, safety, and mechanism of action. *Antimicrob. Agents Chemother.* **57**, 1238–1245 (2013).
41. B. O'Donoghue, K. NicAogáin, C. Bennett, A. Conneely, T. Tiensuu, J. Johansson, C. O'Byrne, Blue-light inhibition of *Listeria monocytogenes* growth is mediated by reactive oxygen species and is influenced by σB and the blue-light sensor Lmo0799. *Appl. Environ. Microbiol.* **82**, 4017–4027 (2016).
42. C. Ayala Orozco, D. Liu, Y. Li, L. B. Alemany, R. Pal, S. Krishnan, J. M. Tour, Visible-light-activated molecular nanomachines kill pancreatic cancer cells. *ACS Appl. Mater. Interfaces* **12**, 410–417 (2020).
43. J.-M. Pagès, C. E. James, M. Winterhalter, The porin and the permeating antibiotic: A selective diffusion barrier in Gram-negative bacteria. *Nat. Rev. Microbiol.* **6**, 893–903 (2008).
44. H. Nikaido, Molecular basis of bacterial outer membrane permeability revisited. *Microbiol. Mol. Biol. Rev.* **67**, 593–656 (2003).
45. M. Lu, S. Wang, T. Wang, S. Hu, B. Bhayana, M. Ishii, Y. Kong, Y. Cai, T. Dai, W. Cui, M. X. Wu, Bacteria-specific phototoxic reactions triggered by blue light and phytochemical carvacrol. *Sci. Transl. Med.* **13**, eaba3571 (2021).
46. P. Ramakrishnan, M. Maclean, S. J. MacGregor, J. G. Anderson, M. H. Grant, Cytotoxic responses to 405 nm light exposure in mammalian and bacterial cells: Involvement of reactive oxygen species. *Toxicol. In Vitro* **33**, 54–62 (2016).
47. C. E. Thurman, A. Muthuswamy, M. M. Klinger, G. S. Roble, Safety evaluation of a 405-nm LED device for direct antimicrobial treatment of the murine brain. *Comp. Med.* **69**, 283–290 (2019).
48. X. Liu, Q. Chang, R. Ferrer-Espada, L. G. Leanse, X. S. Goh, X. Wang, J. A. Gelfand, T. Dai, Photoinactivation of *Moraxella catarrhalis* using 405-nm blue light: Implications for the treatment of otitis media. *Photochem. Photobiol.* **96**, 611–617 (2020).
49. R. S. Gunasekera, T. Galbadage, C. Ayala-Orozco, D. Liu, V. García-López, B. E. Troutman, J. J. Tour, R. Pal, S. Krishnan, J. D. Cirillo, J. M. Tour, Molecular nanomachines can destroy tissue or kill multicellular eukaryotes. *ACS Appl. Mater. Interfaces* **12**, 13657–13670 (2020).
50. N. Ramarao, C. Nielsen-Leroux, D. Lereclus, The insect *Galleria mellonella* as a powerful infection model to investigate bacterial pathogenesis. *J. Vis. Exp.* **70**, e4392 (2012).

51. C. R. Harding, G. N. Schroeder, S. Reynolds, A. Kosta, J. W. Collins, A. Mousnier, G. Frankel, *Legionella pneumophila* pathogenesis in the *Galleria mellonella* infection model. *Infect. Immun.* **80**, 2780–2790 (2012).
52. E. Mylonakis, R. Moreno, J. B. El Khoury, A. Idnurm, J. Heitman, S. B. Calderwood, F. M. Ausubel, A. Diener, *Galleria mellonella* as a model system to study *Cryptococcus neoformans* pathogenesis. *Infect. Immun.* **73**, 3842–3850 (2005).
53. J. C. Junior, B. B. Fuchs, C. P. Sabino, J. C. Junqueira, A. O. C. Jorge, M. S. Ribeiro, M. S. Gilmore, L. B. Rice, G. P. Tegos, M. R. Hamblin, E. Mylonakis, Photodynamic and antibiotic therapy impair the pathogenesis of *Enterococcus faecium* in a whole animal insect model. *PLOS ONE* **8**, e55926 (2013).
54. I. Wojda, Immunity of the greater wax moth *Galleria mellonella*. *Insect Sci.* **24**, 342–357 (2017).
55. G. Jander, L. G. Rahme, F. M. Ausubel, Positive correlation between virulence of *Pseudomonas aeruginosa* mutants in mice and insects. *J. Bacteriol.* **182**, 3843–3845 (2000).
56. A. M. Borman, Of mice and men and larvae: *Galleria mellonella* to model the early host-pathogen interactions after fungal infection. *Virulence* **9**, 9–12 (2018).
57. M. Brennan, D. Y. Thomas, M. Whiteway, K. Kavanagh, Correlation between virulence of *Candida albicans* mutants in mice and *Galleria mellonella* larvae. *FEMS Immunol. Med. Microbiol.* **34**, 153–157 (2002).
58. D. J. Leaper, Silver dressings: Their role in wound management. *Int. Wound J.* **3**, 282–294 (2006).
59. F. D. Halstead, M. Rauf, A. Bamford, C. M. Wearn, J. R. B. Bishop, R. Burt, A. P. Fraise, N. S. Moiemen, B. A. Oppenheim, M. A. Webber, Antimicrobial dressings: Comparison of the ability of a panel of dressings to prevent biofilm formation by key burn wound pathogens. *Burns* **41**, 1683–1694 (2015).
60. M. Guggenheim, R. Zbinden, A. E. Handschin, A. Gohritz, M. A. Altintas, P. Giovanoli, Changes in bacterial isolates from burn wounds and their antibiograms: A 20-year study (1986–2005). *Burns* **35**, 553–560 (2009).
61. Y. Fu, B. Xie, D. Ben, K. Lv, S. Zhu, W. Lu, H. Tang, D. Cheng, B. Ma, G. Wang, S. Xiao, G. Wang, Z. Xia, Pathogenic alteration in severe burn wounds. *Burns* **38**, 90–94 (2012).
62. E. Glukhov, M. Stark, L. L. Burrows, C. M. Deber, Basis for selectivity of cationic antimicrobial peptides for bacterial versus mammalian membranes. *J. Biol. Chem.* **280**, 33960–33967 (2005).
63. G. K. Rajarao, N. Nekhotiaeva, L. Good, Peptide-mediated delivery of green fluorescent protein into yeasts and bacteria. *FEMS Microbiol. Lett.* **215**, 267–272 (2002).
64. J. R. Morones-Ramirez, J. A. Winkler, C. S. Spina, J. J. Collins, Silver enhances antibiotic activity against Gram-negative bacteria. *Sci. Transl. Med.* **5**, 190ra81 (2013).
65. G. A. O'Toole, Microtiter dish biofilm formation assay. *J. Vis. Exp.* **47**, e2437 (2011).
66. L. L. Ling, T. Schneider, A. J. Peoples, A. L. Spoering, I. Engels, B. P. Conlon, A. Mueller, T. F. Schäberle, D. E. Hughes, S. Epstein, M. Jones, L. Lazarides, V. A. Steadman, D. R. Cohen, C. R. Felix, K. A. Fetterman, W. P. Millett, A. G. Nitti, A. M. Zullo, C. Chen, K. Lewis, A new antibiotic kills pathogens without detectable resistance. *Nature* **517**, 455–459 (2015).
67. T. Magoc, D. Wood, S. L. Salzberg, EDGE-pro: Estimated degree of gene expression in prokaryotic genomes. *Evol. Bioinform.* **9**, 127–136 (2013).
68. M. I. Love, W. Huber, S. Anders, Moderated estimation of fold change and dispersion for RNA-seq data with DESeq2. *Genome Biol.* **15**, 550 (2014).
69. X. Ding, C. Yang, W. Moreira, P. Yuan, B. Periaswamy, P. F. de Sessions, H. Zhao, J. Tan, A. Lee, K. X. Ong, N. Park, Z. C. Liang, J. L. Hedrick, Y. Y. Yang, A macromolecule reversing antibiotic resistance phenotype and repurposing drugs as potent antibiotics. *Adv. Sci.* **7**, 2001374 (2020).
70. C. L. Friedrich, D. Moyles, T. J. Beveridge, R. E. W. Hancock, Antibacterial action of structurally diverse cationic peptides on Gram-positive bacteria. *Antimicrob. Agents Chemother.* **44**, 2086–2092 (2000).
71. D. Novo, N. G. Perlmutter, R. H. Hunt, H. M. Shapiro, Accurate flow cytometric membrane potential measurement in bacteria using diethyloxacarbocyanine and a ratiometric technique. *Cytometry* **35**, 55–63 (1999).
72. A. J. O'Neill, K. Miller, B. Oliva, I. Chopra, Comparison of assays for detection of agents causing membrane damage in *Staphylococcus aureus*. *J. Antimicrob. Chemother.* **54**, 1127–1129 (2004).
73. E. C. Carlson, J. L. Audette, N. J. Veitenheimer, J. A. Risan, D. I. Laturnus, P. N. Epstein, Ultrastructural morphometry of capillary basement membrane thickness in normal and transgenic diabetic mice. *Anat. Rec. A Discov. Mol. Cell. Evol. Biol.* **271**, 332–341 (2003).
74. H. Eyring, The activated complex in chemical reactions. *J. Chem. Phys.* **3**, 107–115 (1935).
75. F. Weigend, R. Ahlrichs, Balanced basis sets of split valence, triple zeta valence and quadruple zeta valence quality for H to Rn: Design and assessment of accuracy. *Phys. Chem. Chem. Phys.* **7**, 3297–3305 (2005).
76. M. J. Frisch, G. W. Trucks, H. B. Schlegel, G. E. Scuseria, M. A. Robb, J. R. Cheeseman, G. Scalmani, V. Barone, G. A. Petersson, H. Nakatsuji, X. Li, M. Caricato, A. V. Marenich, J. Bloino, B. G. Janesko, R. Gomperts, B. Mennucci, H. P. Hratchian, J. V. Ortiz, A. F. Izmaylov, J. L. Sonnenberg, D. Williams-Young, F. Ding, F. Lipparini, F. Egidi, J. Goings, B. Peng, A. Petrone, T. Henderson, D. Ranasinghe, V. G. Zakrzewski, J. Gao, N. Rega, G. Zheng, W. Liang, M. Hada, M. Ehara, K. Toyota, R. Fukuda, J. Hasegawa, M. Ishida, T. Nakajima, Y. Honda, O. Kitao, H. Nakai, T. Vreven, K. Throssell, J. A. Montgomery, Jr., J. E. Peralta, F. Ogliaro, M. J. Bearpark, J. J. Heyd, E. N. Brothers, K. N. Kudin, V. N. Staroverov, T. A. Keith, R. Kobayashi, J. Normand, K. Raghavachari, A. P. Rendell, J. C. Burant, S. S. Iyengar, J. Tomasi, M. Cossi, J. M. Millam, M. Klene, C. Adamo, R. Cammi, J. W. Ochterski, R. L. Martin, K. Morokuma, O. Farkas, J. B. Foresman, D. J. Fox, *Gaussian 16, Revision A.03* (Gaussian Inc., 2016).
77. A. L. Santos, V. Oliveira, I. Baptista, I. Henriques, N. C. M. Gomes, A. Almeida, A. Correia, Â. Cunha, Wavelength dependence of biological damage induced by UV radiation on bacteria. *Arch. Microbiol.* **195**, 63–74 (2013).
78. K. Brudzynski, R. Lannigan, Mechanism of honey bacteriostatic action against MRSA and VRE involves hydroxyl radicals generated from honey's hydrogen peroxide. *Front. Microbiol.* **3**, 36 (2012).
79. P. Belenky, J. D. Ye, C. B. M. Porter, N. R. Cohen, M. A. Lobritz, T. Ferrante, S. Jain, B. J. Korry, E. G. Schwarz, G. C. Walker, J. J. Collins, Bactericidal antibiotics induce toxic metabolic perturbations that lead to cellular damage. *Cell Rep.* **13**, 968–980 (2015).
80. D. A. Rowe-Magnus, A. Y. Kao, A. C. Prieto, M. Pu, C. Kao, Cathelicidin peptides restrict bacterial growth via membrane perturbation and induction of reactive oxygen species. *MBio* **10**, e02021–e02019 (2019).
81. R. Dennington, T. A. Keith, J. M. Millam, *GaussView Version 6* (Semichem Inc., 2019).
82. R. E. Stratmann, G. E. Scuseria, M. J. Frisch, Achieving linear scaling in exchange-correlation density functional quadratures. *Chem. Phys. Lett.* **257**, 213–223 (1996).
83. J. Tao, J. P. Perdew, V. N. Staroverov, G. E. Scuseria, Climbing the density functional ladder: Nonempirical meta–generalized gradient approximation designed for molecules and solids. *Phys. Rev. Lett.* **91**, 146401 (2003).
84. S. Grimme, S. Ehrlich, L. Goerigk, Effect of the damping function in dispersion corrected density functional theory. *J. Comput. Chem.* **32**, 1456–1465 (2011).
85. B. I. Dunlap, Robust and variational fitting: Removing the four-center integrals from center stage in quantum chemistry. *J. Mol. Struct. Theochem.* **529**, 37–40 (2000).
86. D. Feller, The role of databases in support of computational chemistry calculations. *J. Comput. Chem.* **17**, 1571–1586 (1996).
87. B. P. Pritchard, D. Altarawy, B. Didier, T. D. Gibson, T. L. Windus, New basis set exchange: An open, up-to-date resource for the molecular sciences community. *J. Chem. Inf. Model.* **59**, 4814–4820 (2019).
88. D. Rappoport, F. Furche, Property-optimized Gaussian basis sets for molecular response calculations. *J. Chem. Phys.* **133**, 134105 (2010).
89. K. L. Schuchardt, B. T. Didier, T. Elsethagen, L. Sun, V. Gurumoorthi, J. Chase, J. Li, T. L. Windus, Basis set exchange: A community database for computational sciences. *J. Chem. Inf. Model.* **47**, 1045–1052 (2007).
90. S. Grimme, J. Antony, S. Ehrlich, H. Krieg, A consistent and accurate *ab initio* parametrization of density functional dispersion correction (DFT-D) for the 94 elements H-Pu. *J. Chem. Phys.* **132**, 154104 (2010).
91. S. Páll, A. Zhmurov, P. Bauer, M. Abraham, M. Lundborg, A. Gray, B. Hess, E. Lindahl, Heterogeneous parallelization and acceleration of molecular dynamics simulations in GROMACS. *J. Chem. Phys.* **153**, 134110 (2020).
92. B. Hess, C. Kutzner, D. Van Der Spoel, E. Lindahl, GROMACS 4: Algorithms for highly efficient, load-balanced, and scalable molecular simulation. *J. Chem. Theory Comput.* **4**, 435–447 (2008).
93. L, Abraham, H. van der Spoel, GROMACS 2020.6 Source code (Zenodo, 2021).
94. S. Jo, T. Kim, V. G. Iyer, W. Im, CHARMM-GUI: A web-based graphical user interface for CHARMM. *J. Comput. Chem.* **29**, 1859–1865 (2008).
95. S. Kim, J. Lee, S. Jo, C. L. Brooks III, H. S. Lee, W. Im, CHARMM-GUI ligand reader and modeler for CHARMM force field generation of small molecules. *J. Comput. Chem.* **38**, 1879–1886 (2017).
96. M. J. Frisch, G. W. Trucks, H. B. Schlegel, G. E. Scuseria, M. A. Robb, J. R. Cheeseman, G. Scalmani, V. Barone, B. Mennucci, G. A. Petersson, H. Nakatsuji, M. Caricato, X. Li, H. P. Hratchian, A. F. Izmaylov, J. Bloino, G. Zheng, J. L. Sonnenberg, M. Hada, M. Ehara, K. Toyota, R. Fukuda, J. Hasegawa, M. Ishida, T. Nakajima, Y. Honda, O. Kitao, H. Nakai, T. Vreven, J. Montgomery Jr., J. E. Peralta, F. Ogliaro, M. Bearpark, J. J. Heyd, E. Brothers, K. N. Kudin, V. N. Staroverov, R. Kobayashi, J. Normand, K. Raghavachari, A. Rendell, J. C. Burant, S. S. Iyengar, J. Tomasi, M. Cossi, N. Rega, J. M. Millam, M. Klene, J. E. Knox, J. B. Cross, V. Bakken, C. Adamo, J. Jaramillo, R. Gomperts, R. E. Stratmann, O. Yazyev, A. J. Austin, R. Cammi, C. Pomelli, J. W. Ochterski, R. L. Martin, K. Morokuma, V. G. Zakrzewski, G. A. Voth, P. Salvador, J. J. Dannenberg, S. Dapprich, A. D. Daniels, Ö. Farkas, J. B. Foresman, J. V. Ortiz, J. Cioslowski, D. J. Fox, *Gaussian 09, Revision D.01* (Gaussian Inc., 2009).
97. S. Jo, T. Kim, W. Im, Automated builder and database of protein/membrane complexes for molecular dynamics simulations. *PLOS ONE* **2**, e880 (2007).
98. S. Jo, J. B. Lim, J. B. Klauda, W. Im, CHARMM-GUI membrane builder for mixed bilayers and its application to yeast membranes. *Biophys. J.* **97**, 50–58 (2009).

99. E. L. Wu, X. Cheng, S. Jo, H. Rui, K. C. Song, E. M. Dávila-Contreras, Y. Qi, J. Lee, V. Monje-Galvan, R. M. Venable, J. B. Klauda, W. Im, CHARMM-GUI *Membrane Builder* toward realistic biological membrane simulations. *J. Comput. Chem.* **35**, 1997–2004 (2014).
100. J. Lee, X. Cheng, J. M. Swails, M. S. Yeom, P. K. Eastman, J. A. Lemkul, S. Wei, J. Buckner, J. C. Jeong, Y. Qi, S. Jo, V. S. Pande, D. A. Case, C. L. Brooks III, A. D. MacKerell Jr., J. B. Klauda, W. Im, CHARMM-GUI input generator for NAMD, GROMACS, AMBER, OpenMM, and CHARMM/OpenMM simulations using the CHARMM36 additive force field. *J. Chem. Theory Comput.* **12**, 405–413 (2016).
101. J. B. Klauda, R. M. Venable, J. A. Freites, J. W. O'Connor, D. J. Tobias, C. Mondragon-Ramirez, I. Vorobyov, A. D. MacKerell Jr., R. W. Pastor, Update of the CHARMM all-atom additive force field for lipids: Validation on six lipid types. *J. Phys. Chem. B* **114**, 7830–7843 (2010).
102. R. M. Venable, A. J. Sodt, B. Rogaski, H. Rui, E. Hatcher, A. D. MacKerell Jr., R. W. Pastor, J. B. Klauda, CHARMM all-atom additive force field for sphingomyelin: Elucidation of hydrogen bonding and of positive curvature. *Biophys. J.* **107**, 134–145 (2014).
103. W. J. Allen, J. A. Lemkul, D. R. Bevan, GridMAT-MD: A grid-based membrane analysis tool for use with molecular dynamics. *J. Comput. Chem.* **30**, 1952–1958 (2009).
104. J. S. Hub, B. L. de Groot, D. van der Spoel, g_wham—A free weighted histogram analysis implementation including robust error and autocorrelation estimates. *J. Chem. Theory Comput.* **6**, 3713–3720 (2010).
105. M. M. Pollard, P. V. Wesenhagen, D. Pijper, B. L. Feringa, On the effect of donor and acceptor substituents on the behaviour of light-driven rotary molecular motors. *Org. Biomol. Chem.* **6**, 1605–1612 (2008).
106. J. Conyard, A. Cnossen, W. R. Browne, B. L. Feringa, S. R. Meech, Chemically optimizing operational efficiency of molecular rotary motors. *J. Am. Chem. Soc.* **136**, 9692–9700 (2014).
107. A. Saywell, A. Bakker, J. Mielke, T. Kumagai, M. Wolf, V. García-López, P.-T. Chiang, J. M. Tour, L. Grill, Light-induced translation of motorized molecules on a surface. *ACS Nano* **10**, 10945–10952 (2016).
108. P.-T. Chiang, J. Mielke, J. Godoy, J. M. Guerrero, L. B. Alemany, C. J. Villagomez, A. Saywell, L. Grill, J. M. Tour, Toward a light-driven motorized nanocar: Synthesis and initial imaging of single molecules. *ACS Nano* **6**, 592–597 (2012).
109. V. García-López, L. B. Alemany, P.-T. Chiang, J. Sun, P.-L. Chu, A. A. Marti, J. M. Tour, Synthesis of light-driven motorized nanocars for linear trajectories and their detailed NMR structural determination. *Tetrahedron* **73**, 4864–4873 (2017).
110. D. Liu, V. García-López, R. S. Gunasekera, L. Greer Nilewski, L. B. Alemany, A. Aliyan, T. Jin, G. Wang, J. M. Tour, R. Pal, Near-infrared light activates molecular nanomachines to drill into and kill cells. *ACS Nano* **13**, 6813–6823 (2019).
111. G. A. Gray, Carbon-13 nuclear magnetic resonance of organophosphorus compounds. VIII. Triphenylphosphoranes and triphenylphosphonium salts. *J. Am. Chem. Soc.* **95**, 7736–7742 (1973).
112. R. S. Reid, The proton NMR spectrum of ascorbic acid: A relevant example of deceptively simple second-order behavior. *J. Chem. Educ.* **66**, 344 (1989).
113. F. Balkau, M. W. Fuller, M. L. Heffernan, Deceptive simplicity in ABMX NMR spectra. I. Dibenzothiophen and 9, 9′-dicarbazyl. *Aust. J. Chem.* **24**, 2293–2303 (1971).
114. J. B. Stothers, C. T. Tan, N. K. Wilson, 13C n.m.r. studies of some phenanthrene and fluorene derivatives. *Org. Magn. Reson.* **9**, 408–413 (1977).
115. J. A. G. Drake, D. W. Jones, High-resolution NMR spectra of fluorene and its derivatives-V ^{1}H and ^{13}C solvent and lanthanide-shift-reagent studies of fluorene-9-one. *Spectrochim. Acta A* **36**, 23–28 (1980).
116. J. Gmach, K. Huben, K. M. Błażewska, α-Fluoro phosphonocarboxylates: The NMR analysis of the heteronuclear ABMX spin system. *Phosphorus Sulfur Silicon Relat. Elem.* **189**, 1216–1225 (2014).
117. R. A. van Delden, N. Koumura, A. Schoevaars, A. Meetsma, B. L. Feringa, A donor–acceptor substituted molecular motor: Unidirectional rotation driven by visible light. *Org. Biomol. Chem.* **1**, 33–35 (2003).
118. V. Diemer, F. R. Leroux, F. Colobert, Efficient and complementary methods offering access to synthetically valuable 1, 2-dibromobenzenes. *Euro. J. Org. Chem.* **2011**, 327–340 (2011).
119. T. N. Murakami, N. Koumura, E. Yoshida, T. Funaki, S. Takano, M. Kimura, S. Mori, An alkyloxyphenyl group as a sterically hindered substituent on a triphenylamine donor dye for effective recombination inhibition in dye-sensitized solar cells. *Langmuir* **32**, 1178–1183 (2016).
120. R. J. Abraham, H. J. Bernstein, The analysis of nuclear magnetic resonance spectra: V. The analysis of deceptively simple spectra. *Can. J. Chem.* **39**, 216–230 (1961).
121. P. Diehl, R. J. Chuck, The analysis of an ABXY N.M.R. spectrum using sub-spectral and direct methods. *Mol. Phys.* **13**, 417–423 (1967).
122. A. Agarwal, J. A. Barnes, J. L. Fletcher, M. J. McGlinchey, B. G. Sayer, Ring currents, local anisotropy, and the problem of the out-of-plane protons: A reinvestigation of the nuclear magnetic resonance spectrum of [10]-paracyclophane. *Can. J. Chem.* **55**, 2575–2581 (1977).
123. T. Kaneda, T. Otsubo, H. Horita, S. Misumi, Layered compounds. LXI. Carbon-13 NMR study of [*n*]-,[*n. n*]-, and multilayered [2.2] paracyclophanes. *Bull. Chem. Soc. Jpn.* **53**, 1015–1018 (1980).
124. J. F. Waters, J. K. Sutter, M. A. B. Meador, L. J. Baldwin, M. A. Meador, Addition curing thermosets endcapped with 4-amino [2.2] paracyclophane. *J. Polym. Sci. Part A Polym. Chem.* **29**, 1917–1924 (1991).
125. J. Lahann, H. Höcker, R. Langer, Synthesis of amino [2.2] paracyclophanes—Beneficial monomers for bioactive coating of medical implant materials. *Angew. Chemie Int. Ed.* **40**, 2947 (2001).
126. G. Ricci, R. Ruzziconi, E. Giorgio, Atropisomeric (*R,R*)-2,2′-Bi([2]paracyclo[2](5,8) quinolinophane) and (*R,R*)-1,1′-Bi([2]paracyclo[2](5,8)isoquinolinophane): Synthesis, structural analysis, and chiroptical properties. *J. Org. Chem.* **70**, 1011–1018 (2005).
127. L. Ernst, V. Boekelheide, H. Hopf, ^{1}H and ^{13}C NMR spectra of multibridged [2$_n$] cyclophanes. *Magn. Reson. Chem.* **31**, 669–676 (1993).
128. L. Ernst, The conformational equilibrium of [2.2] paracyclophanes in solution? *Liebigs Ann./Recl.* **1995**, 13–17 (1995).
129. J. F. Schneider, R. Fröhlich, J. Paradies, Synthesis of enantiopure planar-chiral thiourea derivatives. *Synthesis* **20**, 3486–3492 (2010).
130. M. Dracínsky, P. Jansa, P. Bour, Computational and experimental evidence of through-space NMR spectroscopic J coupling of hydrogen atoms. *Chem. A Eur. J.* **18**, 981–986 (2012).
131. M. K. J. ter Wiel, R. A. van Delden, A. Meetsma, B. L. Feringa, Increased speed of rotation for the smallest light-driven molecular motor. *J. Am. Chem. Soc.* **125**, 15076–15086 (2003).

Acknowledgments: Acknowledgments are due to G. Bennett (BRC, Rice University) for access to laboratory facilities and resources, D. James (Chemistry Department, Rice University) and M. Pena (BRC, Rice University) for technical assistance, R. Butcher and J. Tabor (BRC, Rice University) for access to the microplate reader, M. Meyer (Electron Microscopy Facilities, Rice University) for processing and analysis of samples for electron microscopy, Shared Equipment Authority (SEA) for access to the Sony SA3800 spectral analyzer, W. Chen (Chemistry Department, Rice University) for assistance with the generation of Fig. 1C, and V. García-López for insightful comments and advice. Rice University's Center for Research Computing Night Owls Time-Sharing High Performance Computing Cluster is also acknowledged. Last, we thank the peer reviewers for insightful feedback and constructive criticism. **Funding:** This project has received funding from European Union's Horizon 2020 research and innovation programme under the Marie Skłodowska-Curie grant agreement no. 843116 (to A.L.S.) and the Discovery Institute and the Robert A. Welch Foundation (C-2017-20190330). The funders had no role in the study design, data collection and analysis, decision to publish, or preparation of the manuscript. **Author contributions:** Conceptualization: A.L.S., A.O., G.P.T., and J.M.T. Methodology: A.L.S., D.L., A.v.V., J.L.B., and C.A.-O. Organic synthesis: D.L. and A.v.V. Software: J.T.L., V.D.L., M.M., O.S., and A.B.K. Formal analysis: A.L.S., D.L., A.K.R., A.M.W., J.T.L., V.D.L., M.M., O.S., A.B.K., and L.B.A. Investigation: A.L.S., D.L., and A.v.V. Resources, J.M.T. Writing, original draft: A.L.S., D.L., and A.K.R. Writing, reviewing and editing: A.L.S., D.L., A.K.R., A.M.W., A.v.V., J.T.L., V.D.L., M.M., O.S., A.B.K., J.L.B., C.A.-O., L.B.A., A.O., G.P.T., and J.M.T. Visualization: A.L.S., A.K.R., A.M.W., J.T.L., V.D.L., M.M., O.S., J.L.B., A.B.K., and L.B.A. Supervision: A.B.K., A.O., G.P.T., and J.M.T. Funding acquisition: A.L.S., A.O., G.P.T., and J.M.T. Project oversight: J.M.T. **Competing interests:** Rice University owns intellectual property on the use of electromagnetic (light) activation of MMs for the killing of cells. This intellectual property has been licensed to a company in which J.M.T. is a stockholder, although he is not an officer or director of that company. C.A.-O. is currently an employee in that company. Conflicts of interest are mitigated through regular disclosure to the Rice University Office of Sponsored Projects and Research Compliance. All other authors declare that they have no competing interests. **Data and materials availability:** Bacterial strains and cell lines are commercially available from ATCC and DSMZ. All the necessary details for the synthesis of MMs are provided in the Supplementary Materials. Detailed methods and results from computational analysis of MM parameters are provided in the Supplementary Materials. Other than the specific datasets and analysis code listed below, all data needed to evaluate the conclusions in the paper are present in the paper and/or the Supplementary Materials. The RNA-seq data have been submitted to https://ncbi.nlm.nih.gov/geo/ (GEO accession: GSE194286), and the electron microscopy photographs have been uploaded to https://zenodo.org/ (DOI: 10.5281/zenodo.5888177) and are available.

Submitted 1 September 2021
Accepted 14 April 2022
Published 1 June 2022
10.1126/sciadv.abm2055

ScienceAdvances

Light-activated molecular machines are fast-acting broad-spectrum antibacterials that target the membrane

Ana L. Santos, Dongdong Liu, Anna K. Reed, Aaron M. Wyderka, Alexis van Venrooy, John T. Li, Victor D. Li, Mikita Misiura, Olga Samoylova, Jacob L. Beckham, Ciceron Ayala-Orozco, Anatoly B. Kolomeisky, Lawrence B. Alemany, Antonio Oliver, George P. Tegos, and James M. Tour

Sci. Adv., **8** (22), eabm2055.
DOI: 10.1126/sciadv.abm2055